GEOPHYSICAL CHARACTERIZATIONS OF GLACIAL AQUIFERS

AND EARTH-FILL DAMS

By
MD ZONAED HOSSAIN SAZAL
Bachelor of Science in Geology
University of Dhaka
Bangladesh
2012

Master of Science in Geophysics
University of Dhaka
Bangladesh
2015

Submitted to the Faculty of the
Graduate College of the
Oklahoma State University
in partial fulfillment of
the requirements for
the Degree of
DOCTOR OF PHILOSOPHY
May 2022

GEOPHYSICAL CHARACTERIZATIONS OF GLACIAL AQUIFERS

AND EARTH-FILL DAMS

Dissertation Approved:

Dr. Ahmed Ismail

Dissertation Adviser

Dr. Camelia Knapp

Dr. Daniel A. Laó Dávila

Dr. Rifat Bulut

DEDICATION

In loving memory of my beloved little sister Mukti Bely (2007 – 2021), who was my true inspiration. Thank you for being my lovely little dove, showing me the unconditional love of a sister, and always believing in me. You were the sincere blessing in my life, and you will be loved and remembered till my last breath.

Dedication reflects the views of the author and is not endorsed by committee members or Oklahoma State University.

ACKNOWLEDGEMENTS

First, I would like to convey my heartiest appreciation to my dissertation advisor Dr. Ahmed Ismail, who provided enormous support for completing my Ph.D. degree. His outstanding supervision and guidance in both professional and personal level helped me grow from the apprentice to an ideal researcher. My sincere admiration also goes to Dr. Mohamed Abdelsalam, who was constantly encouraging and enthusiastic. Every time I went to his office, I came out with immense positivity, full of hope and courage I needed.

I want to express my deepest gratitude to my dissertation committee members. Their kind guidance and directions made it happen to complete the dissertation successfully. I thank Dr. Camelia Knapp, who was the role model of prompt action, inspiration, and motivation which always helped me become pro-active. I also thank Dr. Daniel A. Laô Dâvila and Dr. Rifat Bulut for serving my dissertation committee and their suggestions and advice. Thanks to Dr. Jason Thomason for his extensive support and invaluable feedback in my research.

I want to acknowledge Illinois State Geological Survey, Carl Blackwell Dam Authority, and the Grand River Dam Authority for all the necessary support to facilitate this research. I also want to thank Oklahoma State University for the best education and granting me the opportunity for this Ph.D. degree.

I would like to extend my special thanks to all my colleagues, research teammates, and friends, particularly Estefanny, Afshin, Rohit, Ali, Oluseun, Michael, Conn, Evin, Rick, Wakil, Josh, Alejandra, Maria, and Ross. You all motivated me to go through this journey, and thanks for believing in me. I want to thank all the faculties, students, and staff of the Boone Pickens School of Geology for all the technical, teaching, financial, and outreach supports that allowed me to grow up as a professional and achieve my career goal.

My deepest thanks to the friends in the Bangladeshi student community of OSU, particularly Saadbin, Mashfiq, Yeam, Anamul, Shahed, Mahi, Raju, Porom, Belal, Sufia,

Asma, Akib, Sristy, Moushumi, Arif, meem, Nahid, and Sanjida. You made my life brighter, and I appreciate the endless support and the strong bonding we have. I want to recognize my friends from Bangladesh; Abrar, Srezon, Basu, Rajib, Lotus, Bulbul, Rasheek, Rasel, Munim, lal, and Shanto. You always gave me the strength I needed, and I am so lucky to have many friends like you. My Heartiest thanks to the Stillwater Muslim Association for having such a beautiful Mosque within the campus area. I enjoyed the mosque as visiting this place kept replenishing my focus upright.

Finally, I would like to recognize my family sincerely. My respected parents and siblings Himel and Komol always encouraged me to the higher education. Their unconditional love and inspiration constantly kept me robust and motivated for hard work. The endless love and incredible care of my lovely wife Farjana Mily were truly phenomenal throughout these years, which I believe will remain infinite for the blissfully forever.

Thank you.
Md Zonaed Hossain Sazal

Name: MD ZONAED HOSSAIN SAZAL
Date of Degree: MAY, 2022

Title of Study: GEOPHYSICAL CHARACTERIZATIONS OF GLACIAL AQUIFERS AND EARTH-FILL DAMS

Major Field: GEOLOGY

Abstract:

Geophysical investigations of groundwater aquifers and earth-fill dams have gained vast attention during the past few decades. Exploring new groundwater aquifers is always essential to meet the growing need for water resources by the growing population. Investigating dam safety is also crucial as dams store water in lakes and reservoirs and contribute directly to the water supply and flood control. Despite the recent advances in geophysical investigations, delineating complex aquifers and efficient inspection of earth-fill-dams is still challenging. In this study, I conducted and evaluated different geophysical surveys for delineating groundwater aquifers and investigating earth-fill dams. The land streamer shear (S)-wave reflection method was tested in this study as an alternative to traditional geophysical methods for delineating thin and shallow sand and gravel aquifers in northern Illinois. With the aid of available water wells alongside the seismic profiles, the S-wave surveys have successfully resolved multiple sand and gravel aquifers in the surveyed area. The study tested various geophysical methods to investigate the integrity of two earth-fill dams and their underlying rock foundation in central Oklahoma. Tested geophysical methods included seismic P-wave reflection, S-wave reflection, multi-channel analysis of surface wave (MASW), P-wave refraction, and electric resistivity tomography (ERT). The geophysical surveys characterized the different materials and conditions of the two dams and the underlying rock foundations and highlighted the advantages and limitations of the applied geophysical methods. This study introduced the S-wave reflection method as a reliable tool to delineate relatively thin glacial aquifers and evaluated the efficacy of various geophysical methods for investigating earth-fill dams.

TABLE OF CONTENTS

Chapter Page

CHAPTER I: INTRODUCTION 01

1.1 Project Summary 01
1.2 Significance: Intellectual Merits and Broader Impacts 04
1.3 Dissertation Sections 05
References 07

CHAPTER II: SEISMIC SHEAR-WAVE CHARACTERIZATION OF SAND AND GRAVEL GROUNDWATER AQUIFERS IN NORTHERN ILLINOIS 08

2.1 Abstract 08
2.2 Introduction 09
2.3 Geological Setting 12
2.4 Local Correlation of Test Borings 14
2.5 Method and Data Analysis 16
2.1 Data Interpretation 21
2.7 Discussion and Conclusions 30
References 34

CHAPTER III: GEOPHYSICAL CHARACTERIZATION OF THE CARL BLACKWELL EARTH-FILL DAM: STILLWATER, OKLAHOMA, USA 43

3.1 Abstract 43
3.2 Introduction 44
3.3 Site Description and Geology 47
3.4 Data Acquisition 51
3.5 Data Processing 53
3.6 Data Interpretation 57
3.7 Discussion 62
3.8 Conclusion 65
References 67

Chapter Page

CHAPTER IV: GEOPHYSICAL INVESTIGATION OF THE EMBANKMENT PART OF THE KERR DAM, LOCUST GROOVE, OKLAHOMA. 73

4.1 Abstract 73
4.2 Introduction 74
4.3 Site Description and Geology 78
4.4 Method and Data Acquisition 82
4.5 Data Processing 84
4.6 Data Interpretation 86
4.7 Discussion 94
4.8 Conclusion 99
References 102

LIST OF TABLES

Table **Page**

CHAPTER II: Geophysical Characterization of The Carl Blackwell Earth-Fill Dam: Stillwater, Oklahoma, USA

Table 3.1: Acquisition parameters of P-wave and S-wave reflection data..... 53

LIST OF FIGURES

Figure **Page**

CHAPTER I: Seismic Shear-Wave Characterization of Sand and Gravel Groundwater Aquifers in Northern Illinois

Figure 2.1. A map of the study area in northern Illinois shows the acquired five seismic profiles and nearby boreholes and water wells. 11

Figure 2.2. Schematic Cross-section (E–W) of Lithostratigraphic Unit of the study area (Thomason and Keefer, 2013; modified from Curry et al., 1997) 13

Figure 2.3. a) A correlation between Well HEBR-08-01 and HEBR-08-02, and b) their locations 15

Figure 2.4. SH-wave seismic data acquisition using the land streamer system at McHenry County, northern Illinois 16

Figure 2.5. Shear-wave seismic gather from profile 812 showing applied processing steps. a) Raw shot gathers, b) after true amplitude recovery, c) after a bandpass filter, d) after Surface wave noise attenuation, and e) after Predictive deconvolution. 19

Figure 2.6. a) The processed seismic profile 812, and b) the interpreted seismic profile delineating sand and gravel unit of a relatively thick groundwater aquifer 22

Figure 2.7. a) Acquired seismic profile 810, and b) the interpreted seismic profile 810 with a water well showing thick sand and gravel aquifer 24

Figure 2.8. a) Acquired seismic profile 808 without interpretation, and b) with interpretations superimposed 26

Figure 2.9. a) Acquired seismic profile 811 without interpretation, and b) the interpreted seismic profile showing sand and gravel fill deposits 28

Figure 2.10. a) Acquired seismic profile 809, and b) the interpreted seismic profile 809 showing a potential sand and gravel aquifer 29

CHAPTER II: Geophysical Characterization of The Carl Blackwell Earth-Fill Dam: Stillwater, Oklahoma, USA

Figure 3.1. a) A map of the Carl Blackwell dam at the northwest part of the Stillwater, b) A view of the upstream part of the dam, c) A view of the downstream part of the

Figure **Page**

dam, and d) Schematic cross-section A-A' along the dam based on available borehole information. 45
Figure 3.2. a) Modified stratigraphic column showing Permian age deposition within the study area (Petterson, 1933), b) A map showing surficial depositional unit of Quaternary alluvium and Permian bedrock unit of Wellington and Stillwater Formation in the area of Carl Blackwell Lake (Stanley et al., 2008) 49
Figure 3.3. (a) Location of available boreholes along the dam with their lithological description, and (b) the 2-D schematic cross-section A-A' generated using the borehole information
..... 51
Figure 3.4. Location of the collocated geophysical profiles acquired along the crest of the Carl Blackwell dam. The red line marks the location of the geophysical profiles, and BH denotes the borehole locations 52
Figure 3.5. The processing steps of P-wave reflection (left) and S-wave reflection data (right) 54
Figure 3.6. The processing procedure for MALW data involving three steps: a) Acquiring time-domain Love wave data (left panel), b) transforming the time-domain gather to frequency-phase domain and dispersion curve picking (middle panel), and c) Dispersion curve inversion to generate one dimensional velocity-depth profile (right panel) 55
Figure 3.7. a) The Interpreted P-wave (top panel), and interpreted S-wave reflection profile (bottom panel) 58
Figure 3.8. MALW profile (a), and P-wave refraction profile (b) along the embankment of the dam 59
Figure 3.9. The resistivity profile alongside the crest of the dam annotated with interpretations 61
Figure 3.10. a) The ERT profile superimposed on the collocated P-wave reflection profile, b) The interpretation of the MALW profile (black dashed lines) superimposed on the collocated ERT profile, and c) The interpretation of the refraction profile (white dashed lines) superimposed on the collocated ERT profile 63

CHAPTER III: Geophysical Investigation of The Embankment Part of The Kerr Dam, Locust Groove, Oklahoma

Figure 4.1. Map displaying the location of the Kerr dam (a), and the major component of the dam with the study area (b) 79
Figure 4.2. Map of the Ozark uplift area showing the major faults (Seneca and Locust Grove) in the surrounding of the study area (Osborn, 2001) (left). Map showing the

Figure **Page**

dispersion of the geological units within the Ozark uplift area (modified from Cederstrand, 1996a, b) 81
Figure 4.3. Location map of the acquired geophysical data at Kerr dam (a), and locations and description of existing wells (b)..... 84
Figure 4.4. MASW data inversion 86
Figure 4.5. The geophysical profiles acquired along the top of the embankment. a) Schematic drawing of the dam embankment, b) Seismic reflection profile, c) ERT profile, d) MASW profile, and e) seismic refraction profile. Interpreted S-wave seismic interfaces are superimposed on the rest of the geophysical profiles as red dashed lines. Interpreted dashed line with different color indicates the different layers on these profiles. 90
Figure 4.6. The geophysical profiles acquired along the toe of the embankment. a) Schematic drawing of the dam embankment, b) Seismic reflection profile-3, c) ERT profile-1, d) MASW profile-3 and e) Seismic refraction profile-3. Interpreted S-wave seismic interfaces are superimposed on the rest of the geophysical profiles as red dashed lines 93
Figure 4.7. Integrated geophysical profiles along the top of the embankment. a) Schematic drawing of the dam embankment, b) superimposition of Seismic reflection profile and ERT profile, and b) superimposition of seismic reflection profile and MASW profile along the top of the embankment 95
Figure 4.8. Integrated geophysical profiles along the toe of the embankment. a) Schematic drawing of the dam embankment, b) superimposition of Seismic reflection profile and ERT profile, and b) superimposition of seismic reflection profile and MASW profile along the bottom of the embankment 96
Figure 4.9. Combined interpretation of the geophysical data acquired along the top of the embankment (a) and down the embankment (b) of Kerr Dam. 98

CHAPTER I

INTRODUCTION

1.1 Project Summary

Geophysical methods provide non-invasive and cost-efficient solutions for several hydrogeological and geotechnical problems and have gained much attention over conventional methods during the past few decades (Reynolds, 2011; Everett, 2013). However, applications of the geophysical methods need to be continuously evaluated and improved especially for challenging subsurface problems such as imaging glacial aquifers and assessing high-hazard sensitive structures including earth-fill dams. Testing and selecting optimum geophysical methods based on the nature of the geological problem and the conditions of the surveyed site can overcome multiple unfavorable consequences and improve the overall subsurface definition in a time and cost-efficient manner. This study focuses on evaluating and improving the use of geophysical methods for delineating groundwater aquifers and assessing the integrity of earth-fill dams as both dams and aquifers help secure sustainable water resources.

Geophysical delineation of aquifers has been recently developed to meet the increasing demand for new water resources. Delineating groundwater aquifers are traditionally accomplished by drilling boreholes, which is costly and limit the information provided to the locations of the boreholes. Geophysical investigations of groundwater aquifers using electrical and electromagnetic methods also face a challenge at areas with complex geological settings, especially the fine-grained Quaternary and glacial sediments. The high-resolution shear (S)-wave seismic reflection method is applied in this study as an effective alternative to conventional geophysical methods for delineating groundwater aquifers within the complex glacial sediments. This study aimed at testing the feasibility of using high-resolution S-wave reflection method for delineating thin and shallow sand and gravel units, which may comprise potential groundwater aquifers. As S-wave propagation is less affected by the degree of water saturation, available water wells along the seismic surveys provided information about groundwater occurrence within the seismically resolved sand and gravel units.

Geophysical methods are routinely used for dam inspections. Dams act as water barrier for lakes and reservoirs and contributes directly to the water supply, power generation, flood mitigation, and water-based recreation events to the surrounding areas and its ecosystem (Hickey et al., 2015). While dams provide protection and controlled water flow for the nearby area, problems with dams or its underlying foundation may lead over times to potential life-threatening hazard for a mass population. Inadequate monitoring of the dam piping and seepage and foundation defect may trigger eventually cause dam failure (State of Washington, Department of Ecology, 2007). A routine maintenance of dams is necessary

to improve dam safety and prevent dam failure. Geophysical investigations of dams and embankments examine the safety and integrity of the dam structure and its underlying foundation by detecting seepage, internal erosion, or other deficiencies in the dam. Geophysics measure the rock properties such as bulk density; shear module, moisture content, dielectric permittivity, electrical resistivity, which are related to the safety of dams (Adamo et al., 2021). Testing the functionality and applicability of the geophysical methods for dam investigation are essential to ensure their maximum efficiency at different subsurface conditions. Evaluating the geophysical methods for dam investigation and understanding their applicability, advantages and limitation is still poorly constrained. This study is testing and evaluating multiple geophysical techniques at two earth-fill dams in the Oklahoma.

The motivation to pursue this work is that geophysical methods can contribute as a better alternative to traditional investigation techniques for solving groundwater problems as well as dam safety concerns. Evaluating different geophysical methods and highlighting the optimum methods to delineate aquifers and investigate integrity and safety of dam structures are the main goals of this study.

The tested geophysical methods in this study include seismic compressional (P)-wave reflection, SH-wave reflection, P-wave refraction, multi-channel analysis of surface wave (MASW), and electric resistivity tomography (ERT). The results of this study are expected to extend the knowledge about geophysical investigations of sand and gravel aquifers and improve our geophysical characterization of earth-fill dams.

1.2 Significance

Intellectual Merit

This study will enrich the scientific data of the near-surface geophysics discipline by testing and evaluating geophysical methods for aquifer characterization and earth-fill dam investigation. The seismic SH-wave reflection surveys aided by water wells information were evaluated as a promising tool to delineate shallow and thin aquifer units within complex glacial deposits. Evaluating five different geophysical surveys at two dams in this study is necessary to understanding advantages, limitations, and applicability for earth-fill dam investigations in US and other parts of the world. The approach of using combined geophysical techniques is efficient in investigating earth-fill dams and underlying bedrock foundation rock. This study will contribute to the efficient use of non-invasive geophysical techniques for not only the earth-fill dam site investigation but also to routinely monitor the safety and integrity of these dams.

Broader Impact

This study provided high-resolution subsurface imaging of the complex, rapidly varying and thin sand and gravel aquifer units which will contribute to the broad understanding of the hydrogeological systems and to the efforts of securing sustainable drinking water resource for the growing population. Delineating the potential aquifers by this research will impact to the overall knowledge of the groundwater resources in Northern Illinois as the

demand for locating freshwater aquifers has increased dramatically due to the rapidly growing population of Illinois.

This research will also develop the current knowledge about the advantages and limitations of different geophysical methods utilized in dam investigation. There are around 85,000 dams located within USA of which 87% are the earthen dam, corresponding to the National Inventory of Dams (NID, 2009). Maintaining these widely distributed dams need the most efficient and advanced tools for their performance and stability assessment. This study will aid the understanding of selecting the best suite of geophysical methods depending on the type of investigation maximize the success rate of dam assessment. Moreover, the integrated geophysical methods implemented in this study can be used routinely for characterizing dams and help monitor the integrity of the embankment and maintaining its stability for the long run. In broader aspect, this study contribute to the sustainable water resource management as dams directly controls and manage the surface water flow and storage for an area and its surrounding ecosystem.

1.3 Dissertation Sections

This dissertation is defined in three sections. A framework of the dissertation is given below and introduces the three research objectives. The framework also presents the three manuscripts subsequent from this dissertation which are in different phases of the publication.

Paper I: Sazal, Z., Ismail, A., and Thomason, J. (2021). Seismic Shear-Wave Characterization of Sand and Gravel Groundwater Aquifers in Northern Illinois. Journal of Environmental and Engineering Geophysics, 26(3), 183-193. https://doi.org/10.32389/JEEG21-015

Paper II: Sazal, Z., Sanuade, O., and Ismail, A. (2022). Geophysical characterization of the Carl Blackwell earth-fill Dam: Stillwater, Oklahoma, USA. Submitted to Journal of Pure and Applied Geophysics, [Under Review].

Paper III: Geophysical Investigation of the Embankment Part of The Robert S. Kerr Dam, Locust Groove, Oklahoma.

References:

Adamo, N., Al-Ansari, N., Sissakian, V., Laue, J., & Knutsson, S. (2021). Geophysical methods and their applications in dam safety monitoring. Journal of Earth Sciences and Geotechnical Engineering, 11(1), 291-345.

Everett, M. E. (2013). Near-surface applied geophysics. Cambridge University Press.

Hickey, C. J., Römkens, M. J., Wells, R. R., & Wodajo, L. (2015). Geophysical methods for the assessment of earthen dams. In Advances in Water Resources Engineering (pp. 297-359). Springer, Cham.

NID. (2009). National inventory of dams database. http://geo.usace.army.mil/pgis/f?p=397:1:0. Accessed 23 June 2014.

Reynolds, J. M. (2011). An introduction to applied and environmental geophysics. John Wiley & Sons.

State of Washington Department of Ecology. (2007). http://www.ecy.wa.gov/ecyhome.html. Accessed 23 June 2014

CHAPTER II

SEISMIC SHEAR-WAVE CHARACTERIZATION OF SAND AND GRAVEL GROUNDWATER AQUIFERS IN NORTHERN ILLINOIS

2.1 Abstract

Groundwater is a nearly exclusive water source, specifically for the populations which are part of the Chicago metropolitan region. However, water deficiency is anticipated for many communities in this area and need for detecting and delineating groundwater is growing to fulfill the water supply. Shallow sand and gravel aquifers contained by the glacial deposits of the area particularly are high volume aquifer and less stressed in contrast to deeper bedrock aquifer. Yet, these aquifers are poorly recognized in terms of their extent and lateral variability. This research utilized the shear-wave seismic reflection method to delineate the thickness, lateral extent, and internal variability of these aquifers. Horizontally polarized shear-wave (SH-waves) reflection data were obtained alongside five profiles of a total length of 11 km applying the land streamer system in McHenry County in northern Illinois to delineate sand and gravel aquifers. As shear waves transmit through the rock matrix and less susceptible to the presence of water, information from nearby borings and water wells facilitated the interpretation of the obtained SH- wave seismic profiles. Numerous sand and gravel units of prospective aquifers of various thicknesses and lateral extent were

characterized along with the seismic profiles. The comparatively higher vertical and lateral resolution of the shear-waves reflection technique and its less sensitivity to water saturation made it an ultimate method to resolve sand and gravel units of potential aquifers within the complex geological setting if facilitated by water-well data.

2.2 Introduction

McHenry County is situated in the northwest part of Chicago, Illinois. The population of McHenry County is growing very rapidly (Seipel et al., 2016; McKinney, 2011) and is estimated to grow two-fold by 2050 (Northeastern Illinois Planning Commission, 2007). This rapid increase in inhabitants leads to a rise in the demand for water supply, which is a major concern for local planners. McHenry County exclusively depends on groundwater as its sole source of water supply (Carlock et al., 2016; Meyer et al., 2013). Shallow sand and gravel aquifers provide nearly 75% of the public water demand within the region (Lau et al., 2016; Meyer et al., 2013, Berg et al., 1999), whereas deep bedrock groundwater aquifers below glacial deposits provide the rest of the water supply (Berg et al., 1999). Sand and gravel aquifers within McHenry County have been mapped at a regional scale by Curry et al. (1997) and Thomason and Keefer (2013) and are the most productive aquifers in the study area (Meyer et al., 2013).

Detecting and delineating sand and gravel aquifers are traditionally accomplished by interpreting historic drilling records and sometimes drilling several new exploratory boreholes into the potential aquifers.

Drilling boreholes provides high-quality data, but it is costly, and the data are spatially limited. Geophysical imaging has emerged as a more efficient alternative when constrained with boreholes information, which can better detect and delineate sand and gravel aquifers (Thomason et al., 2018). Among the most used geophysical techniques for sand and gravel aquifer exploration is electrical resistivity (ER), electromagnetic (EM), seismic reflection and refraction, ground penetrating radar (GPR) (Hanafy, 2013; Falg`as et al., 2011).

ER methods provide an indirect indication of groundwater presence in hard rock, coarse-grained and clay-free sediments (Muchingami et al., 2012; Ariyo and Banjo, 2008). However, using the method for delineating groundwater becomes very limited within clay-rich and fine-grained glacial deposits. The high moisture content of clay-rich glacial deposits attenuates the EM waves (Beres and Haeni, 1991) and limits the use of EM and GPR methods for groundwater investigation. Seismic methods have been used as an alternative to delineate potential groundwater aquifers (Ahokangas et al., 2020; Maries et al., 2017; Almholt et al., 2013) and image the subsurface with fine-grained deposits within the glacial sediments (Pugin et al., 2009; Guistiniani, 2008; Haines and Ellefsen, 2006).

Seismic refraction is widely used to delineate free water table interface and model aquifer geometries within alluvium and glacial deposits (Gabr et al., 2012). However, this method is less effective when the subsurface is comprised of, for example, alternating low and high seismic-velocity layers as the best results with this method requires increasing seismic velocity with depth (Sjogren, 2013; Abd El-Aal and Mohamed, 2010; Pullan and Hunter, 1990). This low-velocity zone and hidden layer problem is a very common situation

within glacial sediments (Ismail et al., 2014). Additionally, the seismic refraction method typically lacks the necessary vertical resolution to discern thin aquifers at the scale of meters (Bowling et al., 2007). In contrast, seismic reflection methods, including both primary and shear wave, do not require seismic velocity to increase along with depth and provide greater vertical resolution compared to the refraction method (Williams et al., 2005). Therefore, these methods are extensively applied in detecting and delineating shallow groundwater aquifers (Sharpe et al., 2018; Pugin, 2020; Pugin et al., 2014, 2013, 2009; Haines and Ellefsen, 2006).

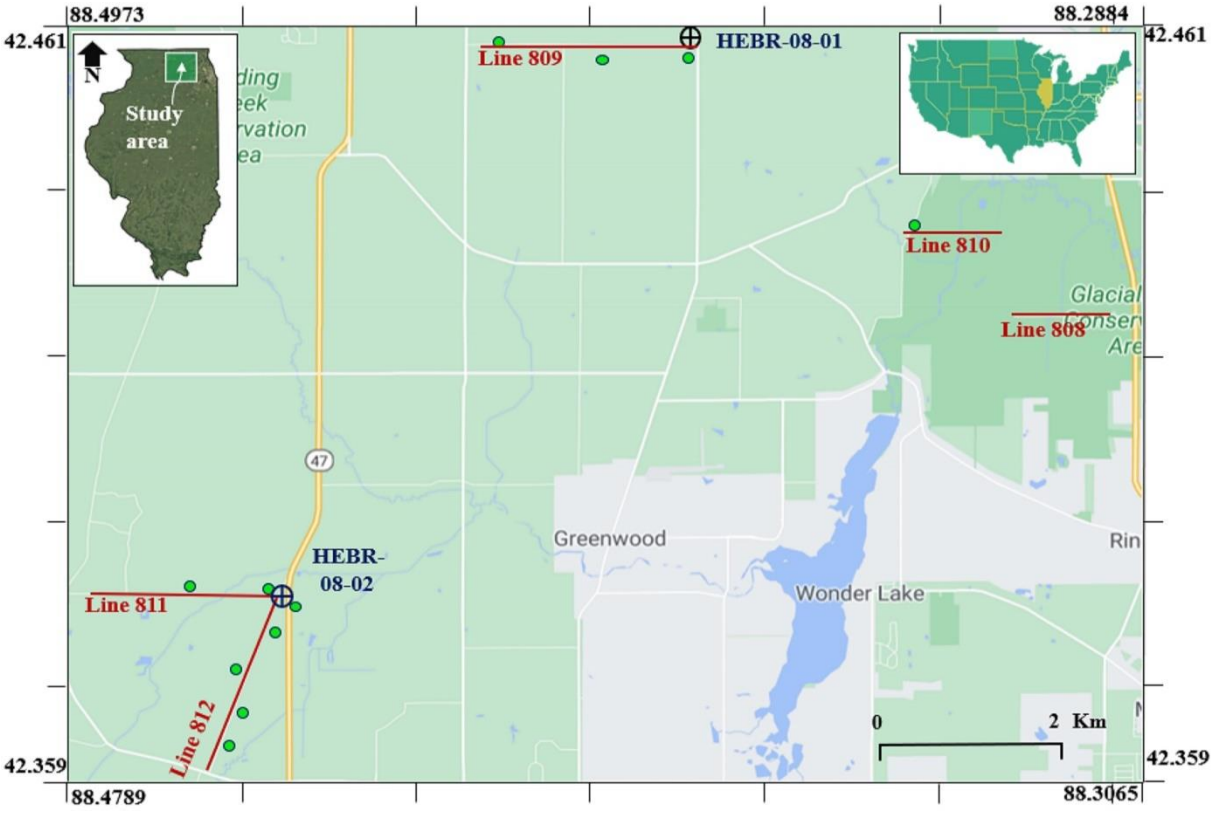

Figure 2.1. A map showing the study area in northern Illinois with acquired five seismic profiles and nearby boreholes and water wells.

The P-wave seismic reflection method is widely used for delineating broad, subsurface sediment architecture, but discerning thin saturated unconsolidated sediments using this method is relatively difficult (Harris, 2009). Gregory (1976) demonstrated that P-wave velocity increases dramatically with rising water content. In contrast, the S-wave velocity remains nearly constant; thus, P-wave energy is quickly attenuated in areas with very shallow groundwater tables. However, many investigations have indicated the value of using S-wave seismic reflection methods to depict shallow, unconsolidated sediments (e.g., Thomason et al., 2018; Pugin et al., 2015; Cox et al., 2006; Woolery et al., 1999), indicating that S-wave reflection method may be more effective for enhanced seismic resolution in contrast to P-wave reflection method (e.g., Harris, 2009). High-resolution S-wave reflection method is used to detect and delineate thin and shallow sand and gravel units that may comprise potential aquifers in McHenry County. The study includes extensive reprocessing of five horizontally polarized shear-wave (SH-waves) profiles and 12 boreholes and water wells (Fig. 2.1) to delineate potential groundwater aquifers. These profiles were previously processed and used along with other geophysical data to build a regional 3D geological model of McHenry County (Thomason et al., 2018; Thomason and Keefer, 2013).

2.3 Geological Setting

The shallow, unconsolidated deposits (up to 100 m thick) within the study region are dominated by interstratified glacial sediments. Multiple glacial events deposited these sediments during the Quaternary Period throughout North America (Fig. 2.2). Older glacial

sediments were often incrementally buried by younger sediments, which resulted in complex glacial sequences that often include alternating beds of clay rich till, lake sediments, and glacial outwash.

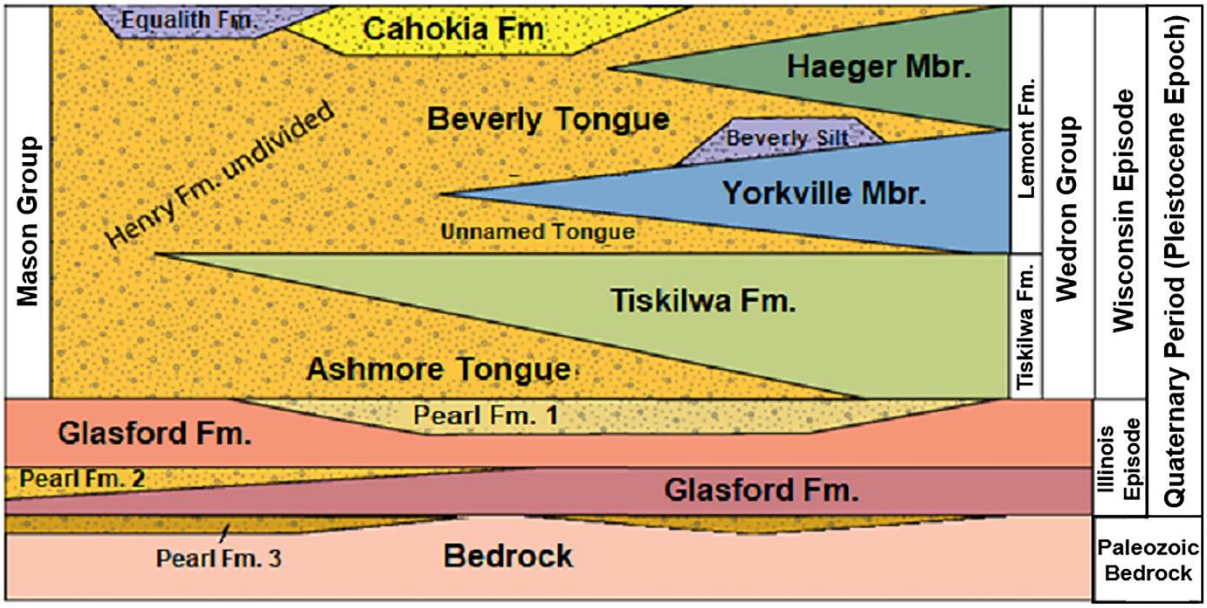

Figure 2.2. Schematic Cross-section (E–W) of Lithostratigraphic Unit of the study area (Thomason and Keefer, 2013; modified from Curry et al., 1997)

A rigorous lithostratigraphic framework for the Quaternary deposits has been developed throughout the study area (Hansel and Johnson, 1996). The framework generally includes deposits that were classified into three sedimentary environments: sub- glacial (till), proglacial fluvial (outwash), and proglacial lacustrine (lake sediments). Lithostratigraphic till units define the relative chronology and distribution of multiple glacial advances in the area. These till units are often bounded vertically and laterally by outwash and lacustrine deposits, and they are typically the bounding aquitard units in aquifer systems. The outwash deposits in the study area are generally either exposed at the land surface or buried beneath till and

lacustrine deposits at depths of up to 100 m. The outwash deposits are generally less than 10 m thick, but locally, their thicknesses can be up to 30 m thick. These outwash sediments are the major sand and gravel aquifer units within the study area, and they are the target of our investigation.

2.4 Local Correlation of Test Borings

An example correlation between local test borings helps better comprehend the variability of lithostratigraphy within the study area which ultimately improve interpretations of the seismic profiles. The lithologic and geophysical logs of two test borings in the area were correlated, which included continuous core samples to bedrock and continuous natural gamma-ray geophysical logs (Fig. 2.3). The correlation of test holes (HEBR-08-01 and HEBR-08-02, Fig. 2.3) shows typical local geologic variability that is often interpreted within the glacial sediments in the study area (Thomason and Keefer, 2013; Curry et al., 1997). In general, the regional lithostratigraphic units (e.g., Mason Group, Lemont Formation, and Tiskilwa Formation) are consistent, identifiable, and mappable. These geologic units are often stratigraphically and lithologically distinctive at any given location. However, given the complexity and glacial depositional systems, geologic units may often be locally absent or spatially variable on the spatial order of kilometers. For example, at site HEBR-08-01, the lithostratigraphy is distinctively marked by a thick succession of Tiskilwa Formation (20 m thick) bounded by Henry Formation (Beverly and Ashmore Members).

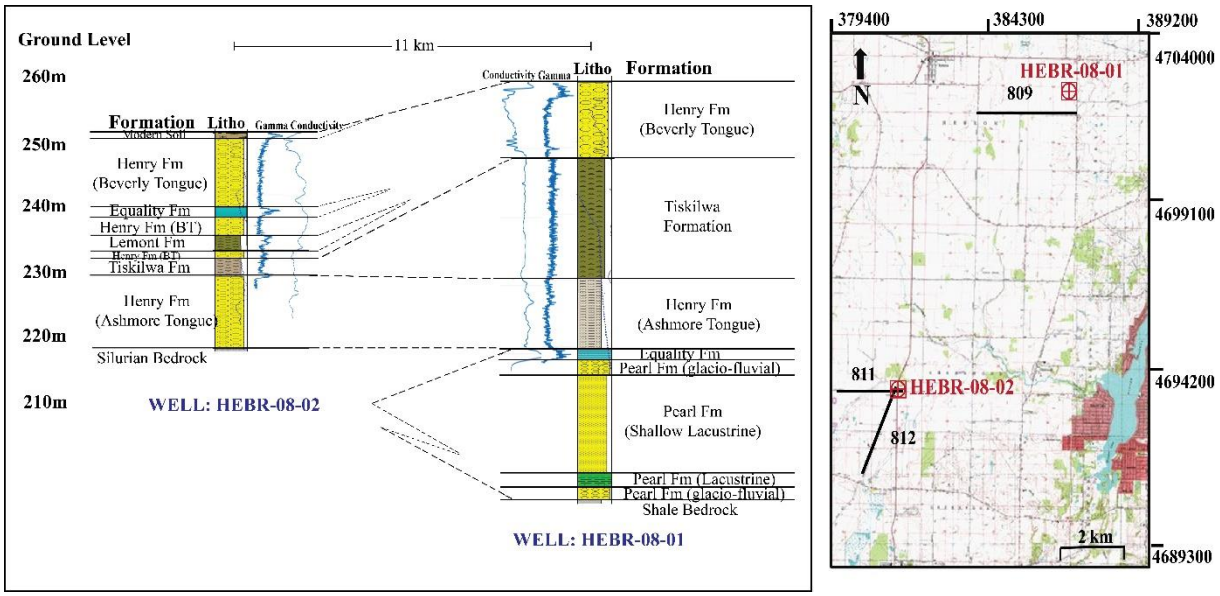

Figure 2.3. a) A correlation between Well HEBR-08-01 and HEBR-08-02, and b) their locations.

Knowledge of the regional geologic framework helped interpret underlying sediments as Illinois Episode Pearl Formation (Thomason and Keefer, 2013). The general stratigraphy of HEBR-08-02 is similar, but the thicknesses of geologic units and the elevation of the bedrock surface are different. For example, the Lemont Formation is present in HEBR-08-02, but it is absent in HEBR-08-01. This is likely a function of local depositional/erosional processes during glaciation and the interpretation that the glaciation that deposited the Lemont Formation did not extend to the location of HEBR-08-01. Nonetheless, the regional geologic stratigraphic framework and expected variability are sufficiently consistent to confidently interpret our seismic profiles.

2.5 Method and Data Analysis

SH-wave reflection methods were utilized exclusively in this study because they provide higher resolution due to shorter wavelengths compared to the same frequency of P-wave (Dobecki, 1988), and the ability to image small-scale subsurface structures facilitates (Omnes, 1978). Also, the SH-wave component has minimum noise of other seismic modes as it does not convert into shear-wave vertical components (SV-wave) or P-wave at layers interfaces (Schuyler- Rossie, 1987). This study used SH-wave seismic- reflection data acquired along five profiles totaling 11 km length using the SH-wave land streamer system (Fig. 2.4).

Figure 2.4. SH-wave seismic data acquisition utilizing the land streamer system at McHenry County, northern Illinois.

The seismic receivers of this system include 24 horizontally polarized geophones of 14-Hz central frequency installed on metal sledges and spaced out at 0.75 m distances. Two SH-wave geophones with opposite horizontal polarity were used at each station. Subtracting the outputs of the two-geophones at each station cancels out the unwanted P-wave arrivals and enhances the SH-wave arrivals (Haines and Ellefsen, 2006; Dobecki, 1988; Schuyler-Rossie, 1987). Impact source (i.e., sledgehammer) and horizontal geophones (axis positioned perpendicular to the seismic profile) were used to generate and record SH-wave. The seismic source is a 2-kg sledgehammer that strikes the horizontal axel of a rolling steel cylinder which is in direct contact with the soil (Pugin et al., 2004). The source and receivers are moved simultaneously at 1.5 m intervals alongside the full extent of each line. Each shot was collected at a 0.5 ms sampling rate and 1.0 s of total recording length using the Geode engineering seismograph. Three seismic shot- gathers were acquired at each source station and vertically stacked to enhance the seismic signal to noise ratio (SNR) in the record. The data were acquired along asphalt roads for better coupling between the geophones and ground surface and to avoid near-surface energy absorption.

The SH-wave data were processed using Landmark ProMax Software. The geometry is assigned to the headers of acquired seismic data considering the locations of the source and receivers (Fig. 2.5(a)) and applied a true-amplitude recovery function to the shot gathers to compensate for the loss of signals' amplitudes with depth caused by attenuation and wavefront spreading. This function uses a time raised to a power correction scheme (g (t) ¼ t POWER, where 't 'and 'POWER' indicates the time and time power constant, respectively) for amplitude adjustment to preserve the relative true amplitude of the signals (Fig. 2.5(b)).

Following the true amplitude recovery, a bandpass filter of 8-12-80-90 Hz was applied to eliminate unwanted frequency within the data (Fig. 2.5(c)). The next processing step focused on eliminating surface waves (Love waves) from the data. Removing the love wave arrivals from the filtered seismic records is essential because Love-waves obscure the SH-wave reflections at the shallow part of the SH-wave records, especially where the near-surface materials are highly compacted. Love waves are the most coherent type of noise for SH-wave methods, and their velocities are closer to the velocities of shear-waves. Therefore, Love waves arrive at nearly the same time as the direct and refracted SH-waves (Haines and Ellefsen, 2006).

The surface-wave noise attenuation (SWNA) module is used within the ProMax processing Software to eliminate Love waves (Fig. 2.5(d)). SWNA uses a low- frequency array, which converts data from time domain to frequency-space domain, performs frequency-dependent mix with the nearby trace, then converts back again to the time-space domain (ProMAX, 1997). The SWNA requires selecting the cut off phase velocity and frequency of the targeted surface waves. Since surface waves in the acquired data attained different phase velocities (180–250 m/s) and frequencies (10–35 Hz), SWNA was applied multiple times with different velocity and frequency values to eliminate a large amount of the surface wave noise (Fig. 2.5(d)). SWNA is applied in common-source domain after splitting it into panels; each panel has a panel size or number of traces, which were selected at seven traces. Traces from adjacent panels are mixed while edge traces are eliminated (ProMAX, 1997). The panels are overlapped and merged after data transformed back from frequency domain to time-domain. Trace scaling was applied before the application of

SWNA to better suppress the noise level and enhance the SH-wave reflection events. Following the SWNA, a predictive deconvolution operator length was determined and employed to the data to eliminate multiples and increase temporal resolution. (Sablon et al., 2011) (Fig. 2.5(e)). Although the data were acquired along relatively flat asphalt roads, elevation correction was applied as the next step to correct for long-wavelength elevation change.

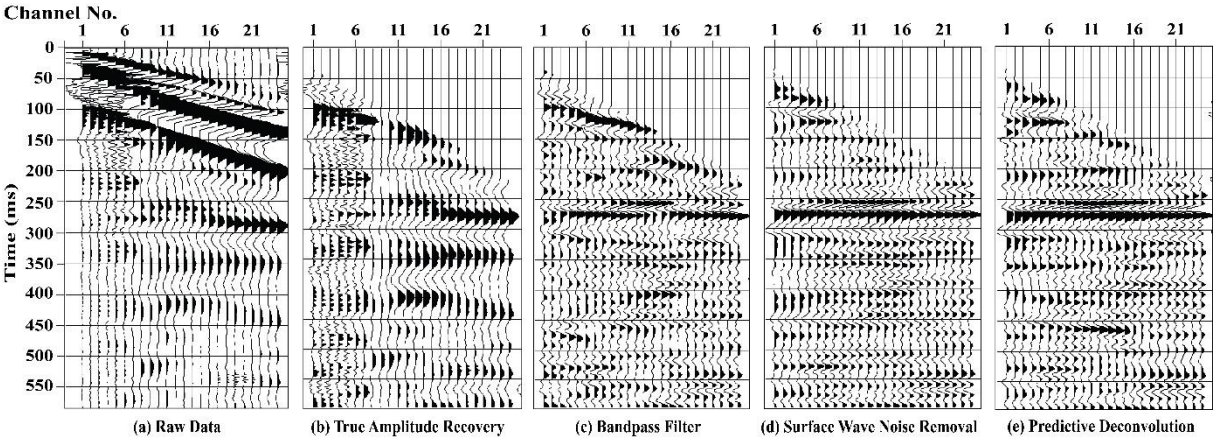

Figure 2.5. Shear-wave seismic gather from profile 812 showing applied processing steps. a) Raw shot gathers, b) after true amplitude recovery, c) after a bandpass filter, d) after Surface wave noise attenuation, and e) after Predictive deconvolution.

Following the elevation correction, a semblance- based velocity analysis was conducted to estimate optimum-stacking velocity functions. The functions will be used as input to the pre-stack time migration process and then convert the stacked seismic profiles from time to depth. The data were migrated using Kirchhoff pre-stack time migration (PSTM). The application of the PSTM to the high-resolution seismic data has recently become a common processing practice and proved to substantially increase the signal-to-noise ratio of seismic

data (Matsushima et al., 2003; Pasasa et al., 1998). In preparation of PSTM, stacking-velocity functions were smoothed along the extent of the seismic profiles, and elevation statics were calculated and applied. Kirchhoff PSTM was applied on the data in the CMP domain and the migrated output was stacked to generate final stacking profiles. A post-stack frequency-space (F-X) deconvolution using Wiener Levinson type filter (Giustiniani et al., 2008) was applied to further improve the coherency of the reflections, eliminate remnant random noise, and increase the lateral continuity of the signal.

Estimating the smallest vertical resolution of the profiles is necessary to understand the limits of interpreting thin aquifer units in our study. Widess (1973) and Yilmaz (2001) have estimated the vertical resolution is a quarter of the seismic wavelength (k). In our study, an estimated peak frequency of 50 Hz was determined along with an average SH-wave seismic velocity (Vs) varying between 260 and 450 m/s within the sediments. This resulted in an estimated vertical seismic resolution limit ranging between 1.3 to 2.6 m. Thus, relatively thin lithological units, similar to those recorded in the test borings, may be resolvable.

Given the estimated vertical resolution, the migrated SH-wave reflection profiles were transformed from time to depth utilizing the smoothed velocity field input to PSTM within the ProMax time-to-depth conversion module. The migrated and depth-converted SH-wave profiles were interpreted to lithological units within the IHS Kingdom software with the aid of boreholes and water well information. The seismic profiles in SEGY format were loaded into the IHS Kingdom software using the coordinates of each seismic trace stored in the seismic file headers. The control wells were also loaded into the software and displayed at

their location along the seismic profiles. Horizon picking started at the locations of the control wells and were completed manually along each seismic profile. The picked seismic horizons were correlated to the control wells and interpreted as interfaces between lithological units.

2.6 Data Interpretation

Five seismic profiles were interpreted separately because the geologic framework at each profile location was relatively unique. The locations of the seismic profiles were selected where the regional geology suggested that shallow sand and gravel aquifers were likely present. Accordingly, seismic profiles were acquired to investigate the local geology in those sites. Twelve water wells/test borings located along the seismic profiles improved their interpretation. Test borings were drilled by the ISGS and included detailed descriptions of lithology and continuous gamma-ray and electrical-conductivity logs. Electrical conductivity logs provide information about clay content and water contents in the geologic units (Schulmeister et al., 2003). Gamma-ray logs also provide information that is, generally, a proxy for clay content, where gamma counts are inversely proportional to particle size (Nazeer et al., 2016). Thus gamma- ray logs help interpret lithologic variability between and within geologic formations. The remaining geologic data were residential water wells that contained reasonable descriptions of the lithology.

Seismic Profile 812

Profile 812 is 2.6 km long and contains 3,441 CMP traces (Fig. 2.6(a)). Five water wells located along the profile have aided the interpretation of this profile (Fig. 2.6(b)) identifying several distinct seismic units. A strong reflector at a depth of ~18 m marks the interface among the uppermost unit (interpreted as surficial Unit A) and the underlying unit that exhibits sub-horizon layering, interpreted as stratified clay (unit B). This contact is consistently observed in the water-well records (Fig. 2.6(b)). A local incised channel was identified at the northeastern side of the profile between 1,750 m and 2,250 m. The horizontal seismic reflections inside the channel suggest that sediments were deposited as flat strata filling the channel (Fig. 2.6(b)).

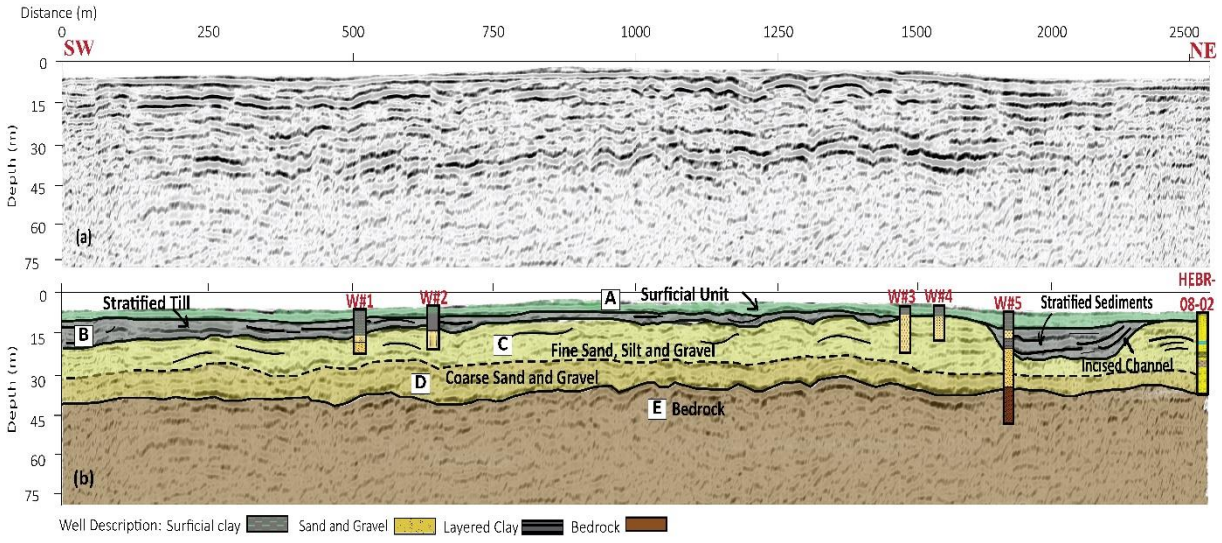

Figure 2.6. The processed seismic profile 812, and b) the interpreted seismic profile delineating sand and gravel unit of a relatively thick groundwater aquifer.

Seismic unit C underlies the stratified upper layer and exhibits flat-lying and weak reflections along the length of the profile. This unit is interpreted as glacial outwash deposits

of sand, silt, and gravel with a thickness of up to 30 m. The low amplitude and less coherent reflections within this unit are most likely due to the high scattering of shear-wave caused by coarse-grained and gravel deposits as indicated by the lithological interpretation of Thomason and Keefer (2013). A moderate to weak, discontinuous reflector exists in the sand and gravel aquifer at a depth of ~30 m from the surface (marked by a dotted line), which may correspond to a change in the grain size or compaction of the sand and gravel deposits at this depth. Such change is not indicated by the available borings. The bedrock surface is recognized as a strong, continuous, and coherent reflector at ~40 m depth (unit E) underlying the interpreted sand and gravel aquifer.

Seismic Profile 810

Profile 810 extends 1.5 km and contains 1,979 CMP traces. Only one water well is located along with this profile (Fig. 2.7(a)). This seismic profile was previously processed and interpreted in Thomason et al. 2018. Our reprocessing and interpretation of the profile shows a flat-lying strong reflector at ~5 m depth is identified as the bottom of an uppermost surficial unit 'A' characterized by thin sub-horizon reflections (Fig. 2.7(b)). This unit attains a varying thickness (5–15 m) and is interpreted as surficial material and stratified clay deposits. A strong and coherent reflector appears at ~15 m depth at the most western part of profile 810 sloping eastward marking the eastern side of a relatively wide incised channel (Fig. 2.7(b)). The western side of the channel was not imaged by the seismic profile 810, which suggests that the channel is likely 1 km wide. The relatively thick channel fill (60–65 m) are characterized as multiple seismic units marks as units B through D with flat-lying and

weak seismic reflections. This channel fill exhibits low amplitude and less coherent reflections and is interpreted as flat layering deposition of sand and gravel glacial outwash. A weak to moderate and discontinuous reflector appeared within the unit at a depth of 30 m, which may be caused through a change in grain size or lithological composition at that depth (Unit C).

A strong, flat-lying, and coherent seismic unit (Unit E) underlying the interpreted sand and gravel unit is recognized at the western side of the profile up to a depth of 40m. This unit exhibits sub-horizon layering and is interpreted as stratified clay as indicated by the water well (Fig. 2.7(b)). The unit holds a maximum thickness of 20 m at the western part of the profile 810 and thins out towards the interpreted incised channel.

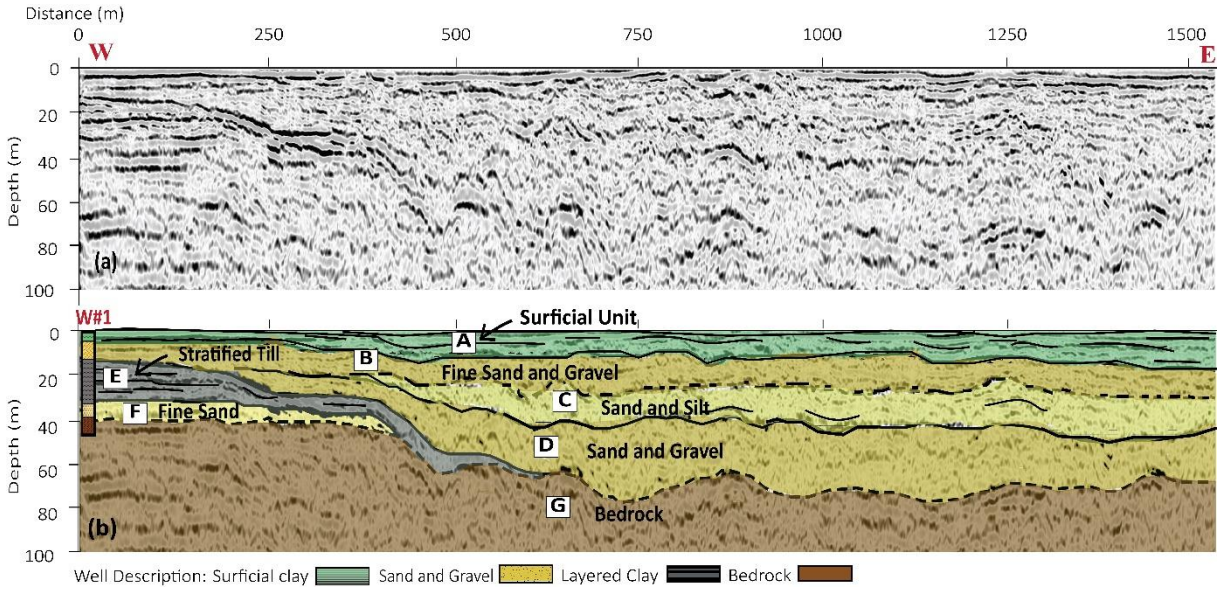

Figure 2.7. a) Acquired seismic profile 810, and b) the interpreted seismic profile 810 with a water well showing thick sand and gravel aquifer

The top of the bedrock (unit G) is identified by a relatively moderate seismic reflector at a depth of 40 m underlying the stratified clay and fine sand units (units E and F) to a weak, discontinuous, and undulated reflector showing at 70 m depth below the sand and gravel channel fill (units B to D). The low amplitude of the bedrock reflector along this line may be due to several aspects of shear-wave energy propagation. The thick and dense glacial till deposits on top of the bedrock (unit E) reflect most of the shear-wave energy and thick sand and gravel deposits attenuate the penetrating shear waves leaving less energy to be reflected off the bedrock surface. Using a lightweight shear wave source in the data acquisition can also limit the shear-wave imaging of the relatively deep bedrock.

Seismic Profile 808

Profile 808 is 1.1 km long and contains 1,450 CMP traces (Fig. 2.8(a)). Test holes and water-well records were unavailable along with this profile, but I relied on the seismic signature of the different glacial sediments interpreted in the other seismic profiles in the study area as well as our knowledge of the geological setting of the region to make reliable interpretation of this profile (Curry et al., 1997; Thomason and Keefer, 2013; Thomason et al., 2018). The upper 15–20 m of profile 808 (Fig. 2.8(b)) shows a series of strong and nearly horizontal seismic reflectors, interpreted as stratified flat-lying silt and clay layers (units A–C). This layer caps a wide incised channel exhibited a strong and continuous seismic reflector which extends along the entire length of the profile and cuts through the glacial deposits down to the bedrock surface among the distance marks of 440 m and 700 m (Fig. 2.8(b)).

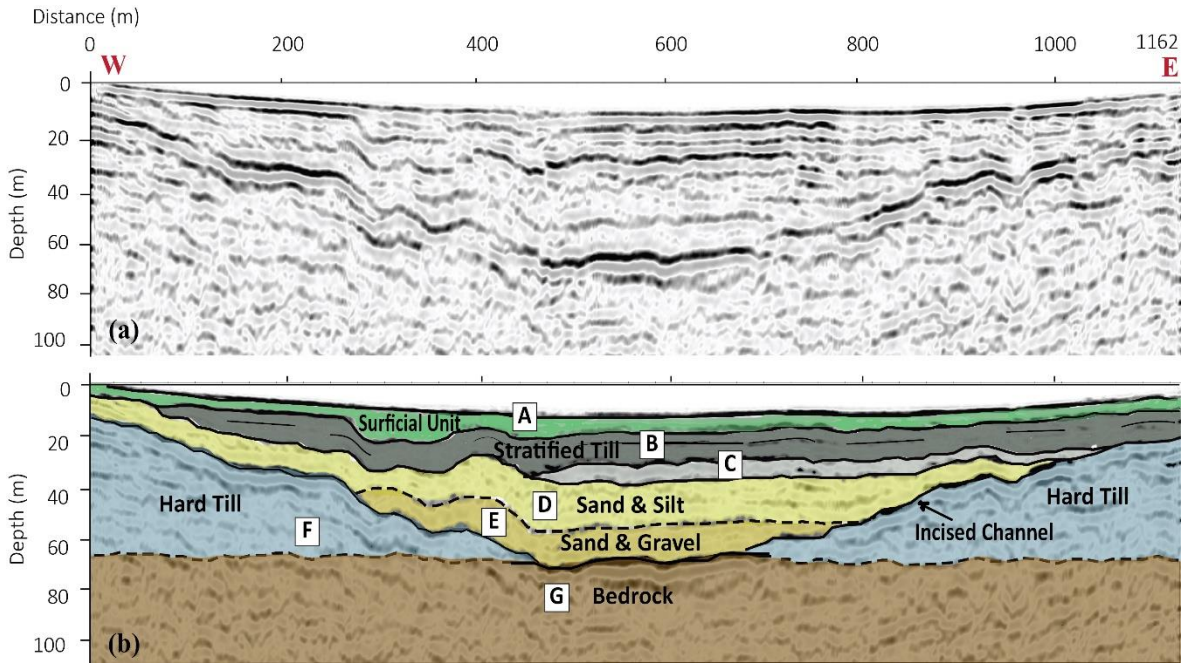

Figure 2.8. a) Acquired seismic profile 808 without interpretation, and b) with interpretations superimposed.

The channel fill deposits, which attains a maximum thickness of 40 m at the center of the channel, are characterized as two flat-lying seismic units with relatively weak seismic reflections, interpreted as an unconsolidated sand layer (unit D) overlying coarse-grained sand and gravel sediments filling the bottom of the channel (unit E). The sand and gravel channel fill deposits have a great potential to be a major groundwater aquifer for this region. The top of the bedrock (unit G) was imaged as a strong seismic reflector only at the bottom of the channel between distances marks of 440–700 m mainly because of the significant seismic impedance difference between the bedrock and overlying coarse sand and gravel channel fill deposits. Away from the base of the channel, the bedrock reflections have dramatically faded mainly because of lack of seismic impedance difference between bedrock

and overlying dense till deposits (Thomason et al., 2018) (unit F), and also because the latter have reflected most of the seismic energy before reaching the bedrock surface.

Seismic Profile 811

Figure 2.9(a) shows a 2 km long seismic profile extending west–east and contains 2700 CMP traces. The two water wells located along the profile were used to aid the interpretation of this seismic profile. A moderate and coherent flat-lying seismic reflector appears at ~8 m depth marks the bottom of the uppermost unit (unit A), interpreted as the surficial unit with clay deposits as indicated by the nearest water well (Fig. 2.9(b)). A strong, coherent, and undulated seismic reflector appears at ~15 m depth marks the bottom of three undulated incised features (Unit B1 to B3), interpreted as stratified hard clay and dense glacial deposits. These incised features B1 to B3 show varying fill thickness of 20 m, 15 m, and 10 m, respectively at the western part of the profile and thin out gradually towards the east. An incised channel (B4) is identified in the eastern part of the profile between distance marks of 1,150 m and 1,450 m. The seismic signature of the channel fill indicates flat layered deposits, interpreted as a sequence of very soft soil, probably lake sediments, as it caused significant seismic energy attenuation.

A low amplitude seismic unit (C) has been identified underlying the stratified hard clay unit. This unit is interpreted as the glacial outwash sediments of sand, silt, and gravel with a maximum thickness of ~20 m. The low amplitude reflections within this unit could be due to the hard glacial clay deposits overlying the unit causing higher energy reflection to the surface and lower energy penetration further deeper. A moderate to weak undulated

reflector at a depth of ~25 m marks the top of another low amplitude seismic unit (Unit D), interpreted as the coarse-grained sand and gravel unit with a thickness of ~10 m along with the profile. Available borehole data supports the sand gravel unit interpretation and identified water table in the wells indicates both sand and gravel units (units C and D) could be interpreted as potential groundwater aquifer. A strong, coherent, and continuous reflector identified at a depth of ~35 m implies the existence of bedrock unit (Unit E) underlying below the sand and gravel aquifer unit.

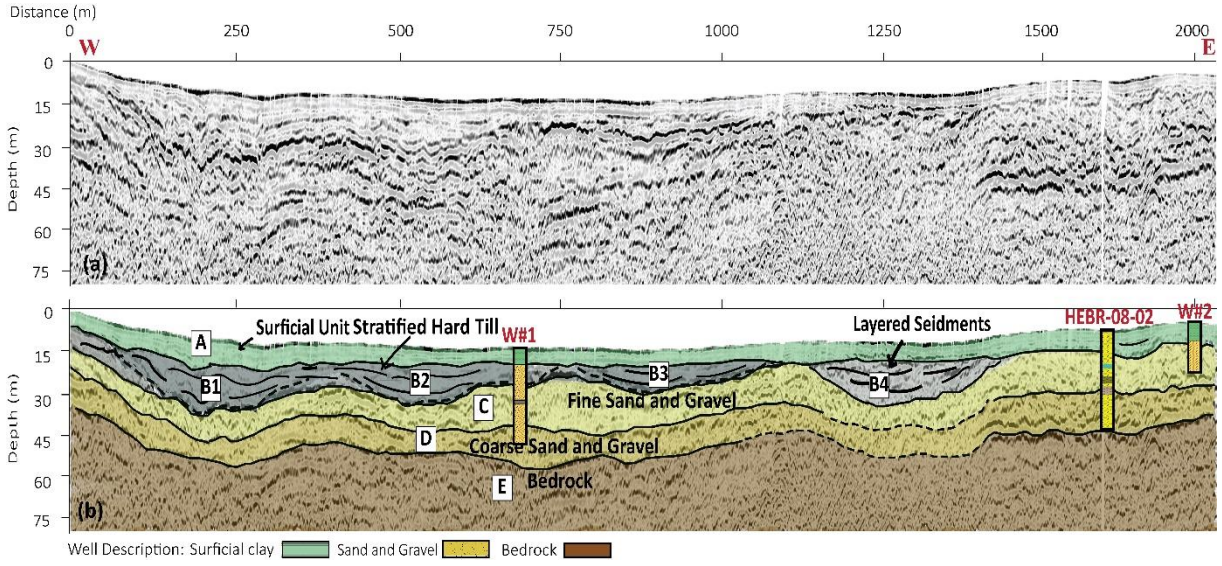

Figure 2.9. a) Acquired seismic profile 811 without interpretation, and b) the interpreted seismic profile showing sand and gravel fill deposits

Seismic Profile 809

Figure 2.10(a) shows a 3.1 km long west-east seismic profile 809 containing 4,000 CMP traces. Four water wells located along the profile have aided the interpretation to resolve potential aquifers (Fig. 2.10(b)). A strong, flat-lying seismic reflector at ~10 m depth marks

the bottom of the uppermost thin surficial unit (A) interpreted as thin clay deposits as observed in the boreholes along with the profile. A relatively thick (30–35 m) seismic unit (B) underlies the upper clay unit and shows low amplitude reflections along the profile, Unit (B) is interpreted as glacial outwash sand and gravel sediments as indicated in the boreholes. The low amplitude reflection of unit (B) could most likely cause by higher energy dissipation from the loosely consolidated, coarse-grained sand and gravel of this unit. Available water table information in all the wells located along the profile falls within this seismically interpreted unit which led us to interpret it as an aquifer within the area. A strong and coherent seismic reflector marks the interface between the bottom of this sand and gravel aquifer unit and an underlying clayey till unit (C) as observed in the boreholes. No seismic reflectors were identified within or below the clayey till deposits unit (C), thus unlike other profiles, the bedrock surface could not be identified confidently in this profile.

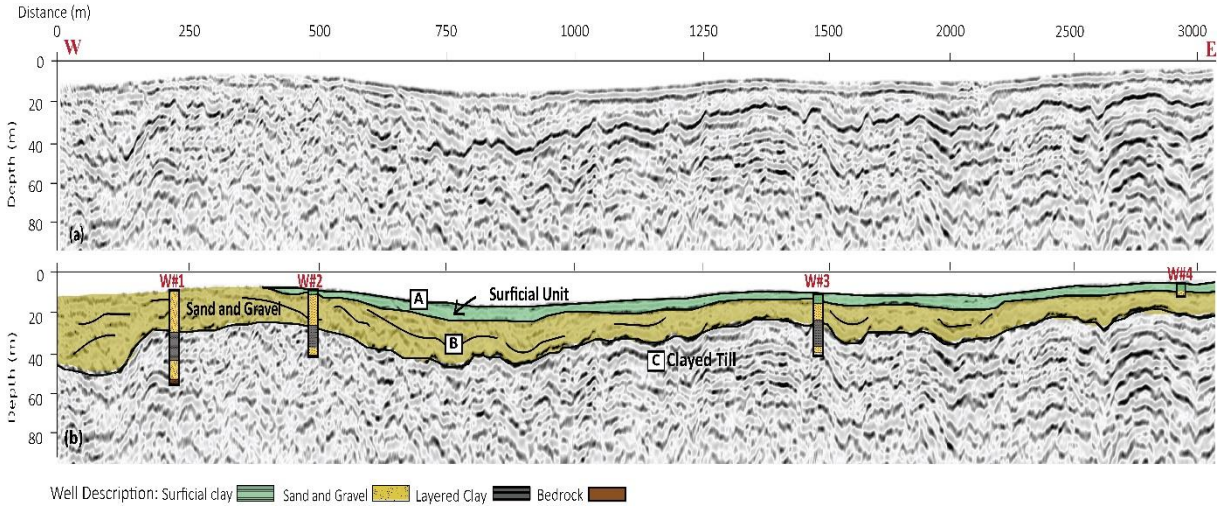

Figure 2.10. a) Acquired seismic profile 809, and b) the interpreted seismic profile 809 showing a potential sand and gravel aquifer

2.7 Discussion and Conclusion

Several studies have used single or multiple geophysical techniques to delineate sand and gravel aquifers in glacial deposits, some of them were successful, and either has met significant challenges. Pugin et al. 2015 used integrated surveys, including P and SH-wave reflection methods, and observed that the P-wave method permits overall seismic facies delineation, but a lesser detailed seismic section compares to SH-wave. However, SH-wave faced difficulties to penetrate deeper and showed higher energy attenuation where thick till deposits were present. Thomason et al. 2018 integrated Electrical Resistivity besides the Seismic Shear-wave reflection method to characterize glacial sediments. However, the Electrical resistivity method was largely ineffective to comprehend the channel morphology and vaguely resolved the internal subsurface features interpreted by the Seismic SH-wave method.

Shear-waves propagation is less susceptible to the existence of water, water saturation, or water chemistry compared to p-waves (Haines and Ellefsen, 2010; Dobecki, 1988), which made the method far from being applied in hydrogeological exploration. However, some groundwater aquifers are present in very complex subsurface settings with relatively variable lateral and vertical distribution, which makes their delineation with surface geophysical methods is a great challenge. For example, delineating the relatively thin and near surface sand and gravel aquifers in the glacial sediments using the electrical and electromagnetic methods is a great challenge (Hanafy, 2013). The P-wave surveys may

produce a strong reflection of the saturated zones that mask further deeper events (Steeples et al., 1997). P-wave propagation is largely influenced by water saturation (Gregory, 1976), has a lower vertical resolution, and may not provide a better image of much shallower subsurface as well as the image of bedrock interface compare to SH-wave. On the contrary, shear-waves are characterized by shorter wavelengths and high resolution, which provide better understandings of the lithology and the pore-fluid distribution, especially for the near-surface area compare to P-wave data alone (Carr et al., 1998).

Applying the shear-waves reflection method in this study enabled to delineate deposits of potential sand and gravel aquifers in shallow depth with their extent, thickness, and lateral lithological variability within the glacial deposits. For instance, the carved features detected in the seismic profile 811 (Fig. 2.9) at less than 35 m depth represent the ability of the SH- wave reflection method to offer thorough information of the architecture and stratigraphy of the overlying sediments on top of the bedrock even at very shallow depth.

Most of the seismic profiles presented in this study showed distinct valley or channel cut features in shallow depth including seismic profiles 812, 810, 808, and 811 (Figs. 2.6, 2.7, 2.8, and 2.9, respectively). The distribution and depositional pattern of the filling of these delineated cut-and-fill valleys or channels features in this study seemed to be nearly identical as the base of the valley was filled by coarse-grained sand and gravel units underlying a thin till or clay layer. The valley fill is capped by surficial topsoil deposits (e.g., profile 810, Fig. 2.7; and profile 808, Fig. 2.8). The resolved channel morphology and stratigraphic boundaries by the Seismic SH-wave reflection method are consistent with

interpretations of other studies of complex glacial deposits (Thomason et al., 2018; Lao et al., 2016; Pugin et al., 2015, 2009).

The results of this research demonstrate that shear- wave reflection surveys can help delineate potential sand and gravel aquifers within complex Quaternary and glacial deposits. Water well information along seismic profile 809 (Fig. 2.10) showed distinct clay and sand layers below the shallow sand and gravel aquifer unit at 30 m depth. However, the seismic profiles could not identify deeper layers along with this profile due to the severe attenuation of the seismic energy below this depth. One possible explanation could be due to a strong reflection event between the aquifer unit and the underlying clay unit so that the majority of the energy has been returned off to the surface. Also, the lightweight source (sledgehammer) was implemented during data acquisition in this study has resulted in a limited depth of penetration.

Despite these limitations, the SH-wave reflection method seemed to be a promising method to delineate shallow aquifers within complex glacial deposits. Along with available geological and geophysical data including water well, this method clearly depicts the near-surface variations and the architecture of the sand and gravel aquifers with their spatial extent and depth along with the seismic profiles. Based on the nature and thicknesses of the seismically delineated aquifers, locations for drilling potentially high-producing and water wells can be suggested along each of the presented seismic profiles.

The central parts of profiles 808 and 812; at distance marks of 800 m, 750 m, and 1,100 m along with profiles 809, 810, and 811, respectively are all good drilling locations where

shallow and thick sand and gravel units were detected. Delineating the potential aquifers by this study contributed to the overall understanding of the groundwater resources in the Northern Illinois as the demand for locating freshwater aquifers has increased dramatically due to the rapidly growing population of Illinois.

References

Abd El-Aal, A.K., and Mohamed, A.A., 2010, Near-surface seismic refraction applied to exploring subsurface clay layer at a new mining area in southeast Cairo, Egypt: Arabian Journal of Geosciences, 3, 105–112.

Ahokangas, E., M˙akinen, J., Artimo, A., Pasanen, A., and Vanhala, H., 2020, Interlobate esker aquifer characterization by high resolution seismic reflection method with landstreamer in SW Finland: Journal of Applied Geophysics, 117, 104014.

Almholt, A., Wiśen, R., Jørgensen, R.B., Ringgaard, J., and Nielsen, U.T., 2013, High resolution 2D reflection seismic land streamer survey for groundwater mapping: Case study from southeast Denmark: in SEG Technical Program Expanded Abstracts 2013, Society of Exploration Geophysicists, 1894–1898.

Ariyo, S.O., and Banjo, A.A., 2008, Application of electrical resistivity method for groundwater exploration in a sedimentary terrain: A case study of Ilara-Remo Southwestern Nigeria: Continental Journal of Earth Sciences, 3, 53–58.

Beres Jr, M., and Haeni, F.P., 1991, Application of ground-penetrating-radar methods in hydrogeologic studies: Groundwater, 29, 375–386. Berg, R.C., Curry, B.B., and Olshansky, R., 1999, Tools for groundwater protection planning: An example from McHenry County, Illinois, USA: Environmental Management, 23, 321–331.

Bowling, J.C., Harry, D.L., Rodriguez, A.B., and Zheng, C., 2007, Integrated geophysical and geological investigation of a heterogeneous fluvial aquifer in Columbus Mississippi: Journal of Applied Geophysics, 62, 58–73.

Carlock, D.C., Thomason, J.F., Malone, D.H., and Peterson, E.W., 2016, Stratigraphy and extent of the pearl-ashmore aquifer, Mchenry County, IL, USA: World Journal of Environmental Engineering, 4, 6–18.

Carr, B.J., Hajnal, Z., and Prugger, A., 1998, Shear-wave studies in glacial till: Geophysics, 63, 1273–1284.

Cox, R.T., Cherryhomes, J., Harris, J.B., Larsen, D., Van Arsdale, R.B., and Forman, S.L., 2006, Paleoseismology of the southeastern Reelfoot rift in western Tennessee and implications for intraplate fault zone evolution: Tectonics, 25.

Curry, B.B., Berg, R.C., and Vaiden, R.C., 1997, Geologic Mapping for environmental planning, McHenry County, Illinois: Illinois State Geological Survey, Champaign, IL, Circular 559.

Dobecki, T.L., 1988, Seismic shear waves for lithology and saturation: in Proceedings of the Second National Outdoor Action Conference on Aquifer Restoration, Groundwater Monitoring and Geophysical Methods, 2, 677–695.

Falg`as, E., Ledo, J., Benjumea, B., Queralt, P., Marcuello, A., Teixiď o, T., and Marť ı, A., 2011, Integrating hydrogeological and geophysical methods for the characterization of a deltaic aquifer system: Surveys in Geophysics, 32, 857–873.

Gabr, A., Murad, A., Baker, H., Bloushi, K., Arman, H., and Mahmoud, S., 2012, September, The use of seismic refraction and electrical techniques to investigate groundwater aquifer, Wadi Alain, United Arab Emirates (UAE): in Conference Proceedings of the Water Resources and Wetlands, 14–16.

Giustiniani, M., Accaino, F., Picotti, S., and Tinivella, U., 2008, Characterization of the shallow aquifers by high-resolution seismic data: Geophysical Prospecting, 56, 655–666.

Gregory, AR., 1976, Fluid saturation effects on dynamic elastic properties of sedimentary rocks: Geophysics, 41, 895–921.

Haines, S.S., and Ellefsen, K.J., 2006, April, Aquifer characterization with seismic shear wave reflection profiling: in 19th EEGS Symposium on the Application of Geophysics to Engineering and Environmental Problems, European Association of Geoscientists & Engineers, cp-181.

Haines, S.S., and Ellefsen, K.J., 2010, Shear-wave seismic reflection studies of unconsolidated sediments in the near surface: Geophysics, 75, B59–B66.

Hanafy, S.M., 2013, March, Groundwater aquifer characterization using geophysical methods: in Symposium on the Application of Geophysics to Engineering and Environmental Problems 2013, Society of Exploration Geophysicists and Environment and Engineering Geophysical Society, 411–414.

Hansel, A.K., and Johnson, W.H., 1996, Wedron and Mason Groups: Lithostratigraphic reclassification of deposits of the Wisconsin episode, lake Michigan lobe area: Illinois State Geological Survey Bulletin, 104, 116.

Harris, J.B., 2009, Hammer-impact SH-wave seismic reflection methods in neotectonics investigations: General observations and case histories from the Mississippi Embayment, USA: Journal of Earth Science, 20, 513.

Ismail, A., Stumpf, A., and Bauer, R., 2014, Seismic characterization of glacial sediments in central Illinois: Journal of Applied Geophysics, 101, 1–10.

Lau, J., Thomason, J.F., Malone, D.H., and Peterson, E.W., 2016, Modeling the sediment fill of the upper Troy pre-glacial Bedrock Valley, McHenry County, Illinois, USA: Journal of Geoscience and Environment Protection, 4, 107–122.

Maries, G., Ahokangas, E., M˙akinen, J., Pasanen, A., and Malehmir, A., 2017, Interlobate esker architecture and related hydrogeological features derived from a combination of high-resolution reflection seismics and refraction tomography, Virttaankangas, southwest Finland: Hydrogeology Journal, 25, 829–845.

Matsushima, J., Okubo, Y., Rokugawa, S., Yokota, T., Tanaka, K., Tsuchiya, T., and Narita, N., 2003, Seismic reflector imaging by prestack time migration in the Kakkonda geothermal field, Japan: Geothermics, 32, 79–99.

McKinney, C., 2011, Update on water studies groundwater protection program: Division of Water Resources, County of McHenry.

Meyer, S.C., Roadcap, G.C., Lin, Y.F., and Abrams, D.B., 2013, Groundwater simulation modeling and potentiometric surface mapping, McHenry County, Illinois: ISWS Contract Report CR-2013-06.

Muchingami, I., Hlatywayo, D.J., Nel, J.M., and Chuma, C., 2012, Electrical resistivity survey for groundwater investigations and shallow subsurface evaluation of the basaltic-greenstone formation of the urban Bulawayo aquifer: Physics and Chemistry of the Earth, Parts A/B/C, 50, 44–51.

Nazeer, A., Abbasi, S.A., and Solangi, S.H., 2016, Sedimentary facies interpretation of Gamma Ray (GR) log as basic well logs in Central and Lower Indus Basin of Pakistan: Geodesy and Geodynamics, 7, 432–443.

Northeastern Illinois Planning Commission (NIPC), 2007, Northeastern Illinois Planning Commission endorsed 2030 forecasts revised: Northeastern Illinois Planning Commission, Chicago, IL.

Omnes, G., 1978, Exploring with SH-waves: Journal of the Canadian Society of Exploration Geophysics, 14, 40–49.

Pasasa, L., Wenzel, F., and Zhao, P., 1998, Pre-stack Kirchhoff depth migration of shallow seismic data: Geophysics, 63, 1241–1247.

ProMAX, 1997, A reference guide for the ProMAX geophysical processing software. Landmark, a Halliburton Company. Volume 2

Pugin, A.J.M., 2020, SS and PP high-resolution seismic reflection applied to near surface mapping: in Fifth International Conference on Engineering Geophysics (ICEG), Society of Exploration Geophysicists, 111–114.

Pugin, A.J.M., Crow, H., Bajc, A.F., and Rainsford, D.R., 2015, March, Multicomponent vibroseismic profiling over high velocity glacial ground: an example from southern Ontario: in Symposium on the Application of Geophysics to Engineering and Environmental Problems, Society of Exploration Geophysicists and Environment and Engineering Geophysical Society, 478–484.

Pugin, A.J.M., Oldenborger, G.A., Cummings, D.I., Russell, H.A., and Sharpe, D.R., 2014, Architecture of buried valleys in glaciated Canadian Prairie regions based on high resolution geophysical data: Quaternary Science Reviews, 86, 13–23.

Pugin, A.J.M., Brewer, K., Cartwright, T., Pullan, S.E., Perret, D., Crow, H., and Hunter, J.A., 2013, Near surface S-wave seismic reflection profiling–new approaches and insights: First Break, 31.

Pugin, A.J.M., Pullan, S.E., Hunter, J.A., and Oldenborger, G.A., 2009, Hydrogeological prospecting using P-and S-wave land streamer seismic reflection methods: Near Surface Geophysics, 7, 315–328.

Pugin, A.J.M, Larson, T.H., Sargent, S.L., McBride, J.H., and Bexfield, C.E., 2004, Near- surface mapping using SH-wave and P-wave seismic land-streamer data acquisition in Illinois, US: The Leading Edge, 23, 677–682.

Pullan, S.E., and Hunter, J.A., 1990, Delineation of buried bedrock valleys using the optimum offset shallow seismic reflection technique: in Ward, S.H. (Ed.), Geotechnical and Environmental Geophysics, Geotechnical, Society of Exploration Geophysicists, 3, 75–87.

Sablon, R., Russier, D., Zurita, O., Hardouin, D., Gratacos, B., Soubaras, R., and Lin, D., 2011, Multiple attenuation for variable-depth streamer data: from deep to shallow water: in SEG Technical Program Expanded Abstracts, Society of Exploration Geophysicists, 3505–3509.

Schulmeister, M.K., Butler Jr, J.J., Healey, J.M., Zheng, L., Wysocki, D.A., and McCall, G.W., 2003, Direct-push electrical conductivity logging for high-resolution hydrostratigraphic characterization: Groundwater Monitoring & Remediation, 23, 52–62.

Schuyler-Rossie, C., 1987, The seismic refraction compression-shear wave velocity ratio as an indicator of shallow water tables, a field test, Army engineer waterways experiment station Vicksburg MS environmental lab: Military Hydrology, Report 15.

Seipel, L.C., Peterson, E.W., Malone, D.H., and Thomason, J.F., 2016, Role of multiple high capacity irrigation wells on a surficial sand and gravel aquifer: Journal of Geoscience and Environment Protection, 2016, 4, 43–53.

Sharpe, D.R., Pugin, A.J.M., and Russell, H.A., 2018, Geological framework of the Laurentian trough aquifer system, southern Ontario: Canadian Journal of Earth Sciences, 55, 677–708.

Sjogren, B.(Ed.)., 2013, Shallow refraction seismics: Springer Science & Business Media.

Steeples, D.W., Green, A.G., McEvilly, T.V., Miller, R.D., Doll, W.E., and Rector, J.W., 1997, A workshop examination of shallow seismic reflection surveying: The Leading Edge, 16, 1641–1647.

Thomason, J.F., and Keefer, A.K., 2013, Three-dimensional geologic mapping for Mchenry County: Illinois State Geological Survey Contract Report.

Thomason, J.F., Larson, T.R., Ismail, A., and Sargent, S., 2018, Characterizing glacial sediments and features in northeast Illinois using electrical resistivity and seismic-reflection profiling: Quaternary Glaciation of the Great Lakes Region: Process, Landforms, Sediments, and Chronology, 530, 233.

Widess, M.B., 1973, How thin is a thin bed?: Geophysics, 38, 1176–1180.

Williams, R.A., Stephenson, W.J., Odum, J.K., Worley, D.M., Asten, M.W., and Boore, D.M., 2005, P-and S-wave seismic reflection and refraction measurements at CCOC, Blind Comparisons of Shear-Wave Velocities at Closely Spaced Sites in San Jose, California, 1169.

Woolery, E.W., Street, R.L., Wang, Z., Harris, J.B., and Mclntyre, J., 1999, Neotectonic structure in the central New Madrid seismic zone: Evidence from multimode seismic-reflection data: Seismological Research Letters, 70, 554–576.

Yilmaz,¨O., 2001, Seismic data analysis: Processing, inversion, and interpretation of seismic data: Society of exploration geophysicist.

CHAPTER III

GEOPHYSICAL CHARACTERIZATION OF THE CARL BLACKWELL EARTH-FILL DAM: STILLWATER, OKLAHOMA, USA

3.1 Abstract

Multiple non-intrusive geophysical surveys were conducted along the crest of earth-fill Carl Blackwell Dam in Stillwater, Oklahoma, in order to characterize the body of the dam, the soil and rocks of the dam foundation, and zones of potential seepage or internal erosion. The geophysical surveys included seismic P- and S-wave reflections, multichannel analysis of Love wave (MALW), P-wave refraction, and electrical resistivity tomography (ERT). Integrating the results of the geophysical surveys has successfully characterized the dam body into upper and lower dam fill units and identified a low S-wave velocity and resistivity zone interpreted as a zone of potential seepage or internal erosion. The results also delineated the top of the foundation soil and foundation rock and imaged a local bedrock valley cutting through the sandstone foundation rock down to an underlying shale unit. This study showed how the efficient the integration of seismic and electrical methods can better characterize dams and underlying foundations.

3.2 Introduction

The effectiveness of the safety evaluation of the larger infrastructures i.e., dams is controlled mainly by understanding the mechanical parameters and subsurface conditions of the structures. Most of the dams in the country have exceeded the proposed initial plan, and thus their mechanical properties may have degraded and become a significant concern (Karastathis et al., 2002; Bond et al., 2000). Aging is one of the factors that can cause dam failure, and distinctive measures may be needed to reduce the risk of dam failure by assessing their foundations and underlying subsurface conditions (Nwokebuihe et al., 2017). The Carl Blackwell dam in Stillwater, Oklahoma, is an earth-fill structure that has been classified by the National Inventory of Dams (NID) in 2018 as a high hazard potential yield dam. The basis of this classification is the assessment of the expected impact of a potential dam failure (Hickey et al., 2015).

The dam has greatly exceeded its economic lifetime, which was planned for 50 years according to the Soil Conservation Service (SCS) during the construction of the earthen dam (Hickey et al., 2015). Therefore, for Carl Blackwell dam being a near century-old dam, it is pertinent to investigate its integrity, especially with the recent increase in seismic activities in Oklahoma. Moreover, the recently delineated Lake Carl Blackwell (LCB) fault near the center of the Carl Blackwell Lake (Jaiswal et al., 2019 and Darold and Holland 2015) may be a potential hazard to the safety of the dam. Moreover, rodent burrows features observed in the downstream side of the Carl Blackwell dam (Amec, 2015) may provide seepage pathways leading to potential piping, which can significantly threaten the dam's integrity. Therefore, routine investigation of the Carl Blackwell dam is crucial to monitor its integrity and stability.

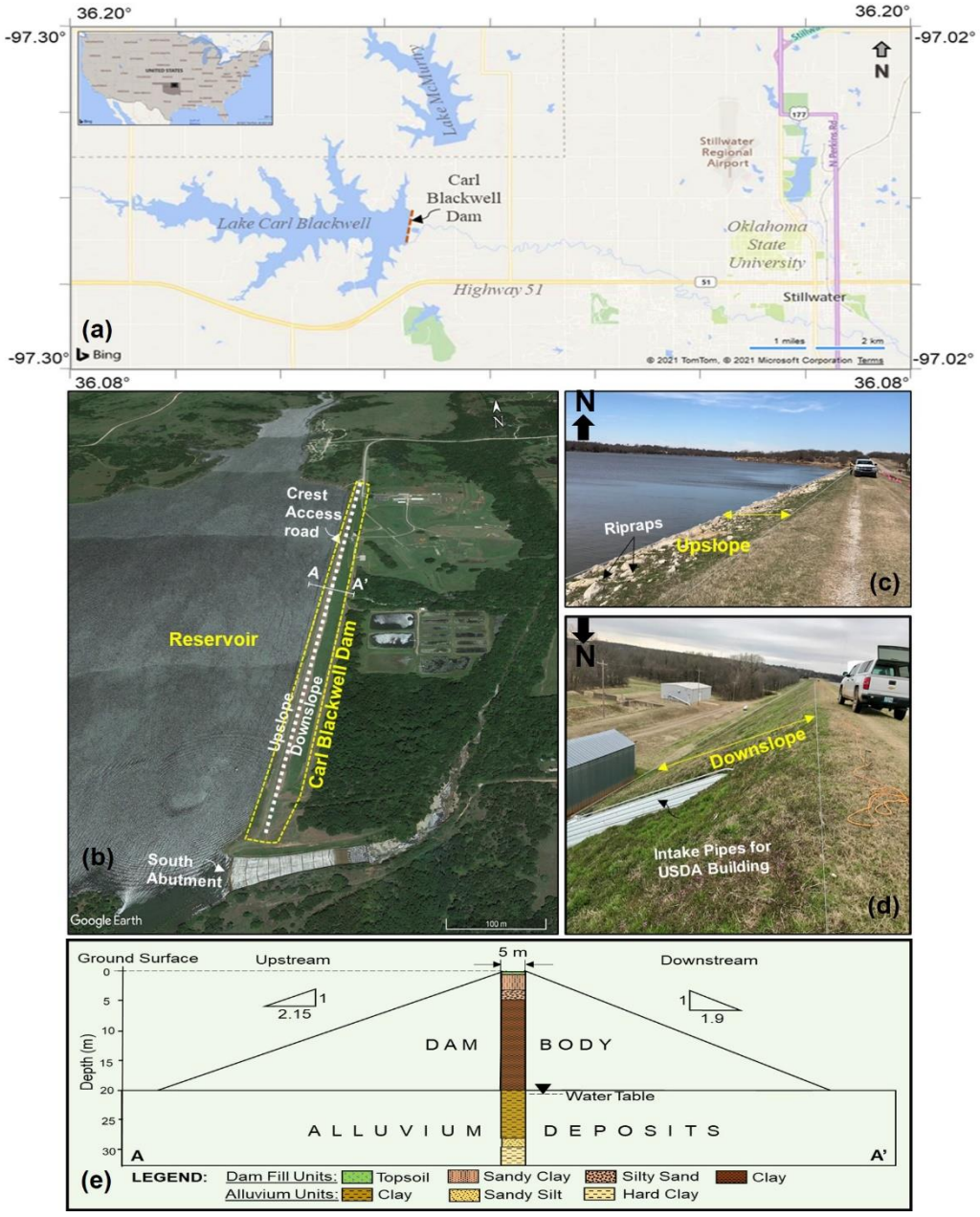

Figure 3.1. a) A map of the Carl Blackwell dam at the northwest part of the Stillwater, b) A view of the upstream side of the dam, c) A view of the downstream side of the dam, and d) Schematic cross-section A-A' along the dam based on available borehole information.

Dam investigation has traditionally relied on geotechnical engineering measurements, including standard penetration tests (SPT) and cone penetration tests (CPT) (Abdulsamad et

al., 2019; Woolery 2018). These traditional methods are invasive, lack required resolution, and often require drilling holes, which are intrusive and relatively expensive (Woolery, 2018). Drilling holes through the body or the dam foundation rock may lead to seepage and piping and eventually causes dam failure (Stare et al., 2012).

Recently, geophysical methods have been used as a more efficient alternative to investigate dams by delineating the geometry of the dam body (Cardarelli et al., 2014), detecting potential seepage through or under the dam (Carnevale et al., 2011), and imaging dam foundations (Hunter et al., 2007). The seismic compressional (P) and shear wave (S) reflection methods can successfully image subsurface units, structures, bedrock interfaces, and different embankment units (Inazaki, 2007, Ismail, et al., 2017). The multichannel analysis of surface waves (MASW) method is applied to measure the S-wave velocity (Vs) variability in near-surface (Ismail et al., 2014). Measuring Vs variation in the subsurface is significant to determine low strain elastic properties of dams' internal core, which can be used to estimate the stability and integrity of the dam (Park and Kishida, 2018; Cardarelli et al., 2014, 2010). The seismic P-wave refraction measures the velocity (Vp) of P-wave of the subsurface and can indicate weak zones within the body of dams (Avalos et al., 2016; Saad et al., 2013).

However, applying a single geophysical method for dam investigation may not deliver a reliable evaluation of the dam (Dezert et al., 2019). Instead, applying two or more complementary methods provides better characterization of dams and reduces non-uniqueness in interpreting geophysical data (Ikard et al., 2015; Cardarelli et al., 2014;

Cardarelli et al., 2010; Hunter et al., 2007). For instance, the seismic methods offer knowledge about the mechanical properties of the subsurface. In contrast, electrical techniques indicate zones of infiltration or seepages and can be used to monitor fluid-induced variation. Therefore, integrating these both methods are applied to characterize the integrity of the foundation rocks, potential seepage, and preferential flow pathway inside the dam structure (Sazal et al., 2021; Sjödahl et al., 2008). Though, evaluating the efficiency, sensitivity, and limitation of geophysical methods applied to dam investigations will help select the optimum geophysical methods to better understand the geotechnical and engineering problems of dams. In this research, seismic P- and S-wave reflection, multichannel analysis of Love wave (MALW), P-wave refraction, and electrical resistivity tomography (ERT) were implemented to investigate the body of the Carl Blackwell dam, the underlying foundation soil and rocks, and potential seepage zones with internal erosion. This study also aims to evaluate integrating the electrical and seismic methods for earth-fill dam investigations.

3.3 Site Description and Geology

The Carl Blackwell dam is located on the easternmost part of a mid-sized lake named Carl Blackwell at the northwestern part of the city of Stillwater in Payne County, Oklahoma (Fig. 3.1a). The Carl Blackwell Dam was built in 1937 along Stillwater creek with an utmost water capacity about 7.5 million cubic meters (Oklahoma Water Resources Board, 2020). The crest of the dam is 1210 m long with 22 m average dam height. The principal spillway of the

dam consists of an ogee weir with a concrete channel and is located at the south abutment (Fig. 3.1b). An access road passes on the dam crest all the way up to the principal spillway. The dam's upstream side is covered by ripraps consisting of rock fragments and concrete blocks (Fig. 3.1c), while the downstream side is covered by soil and vegetation. A water intake structure belonging to the United States Department of Agriculture (USDA) is located at the dam's downstream side at around 320 m from the northern abutment to supply water to their research facility (Fig. 3.1d). This earthen dam structure was built on a nearly horizontal layer made of quaternary alluvium deposits of different grain sizes (Fig. 3.1e).

Geologically, this area is part of the eastern flank of Nemaha Uplift. Several uplift events bounded the area, including Arkoma basin in the southeast, Arbuckle Mountain in the south, Wichita uplift to the southwest, Anadarko basin in the west, and Cherokee platform east (Northcutt and Campbell, 1998). A prominent east-west trending Lake Carle Blackwell (LCB) fault was detected in the deep Mississippian formation near the dam (Jaiswal et al., 2019). The direction of sediment deposition is east-west, with shallow water sediments being widespread on the carbonate shelf in the northern part of the area (LeBlanc, 2014).

The dam is underlain by Quaternary alluvium and Permian bedrock units (Fig. 3.2a). The Quaternary deposits are characterized as loosely compacted and unconsolidated sediments (Stanley et al., 2008; Fig. 3.2b). Such sediments mainly consist of clay, silt, sand, and gravel, deposited by a modern stream of a fluvial system (Adams and Bergman, 1996). The bedrock underlying the alluvial deposits unit is of Permian age and consists of Wellington and Stillwater Formation. The Wellington Formation mainly includes the Upper Iconium Member

and Lower Fallis Member. The upper portion of the Wellington Formation is dominantly shaly (Iconium Member) with interbedded sandstone, and the lower part of the Formation is mostly sand (Fallis Member). However, the Fallis member contains more interstratified shale and sandstone, with the shale becoming more dominant to the west (Petterson, 1933). The Stillwater Formation consists of shale, sandstone, and dolomitic conglomerate gradually changing from predominant sand to predominant shale towards the top of the Formation. The gradation of sand to shale is slow, with a distinct break between the Fallis Sandstone and the top of the Shaly Stillwater Formation (Petterson, 1933).

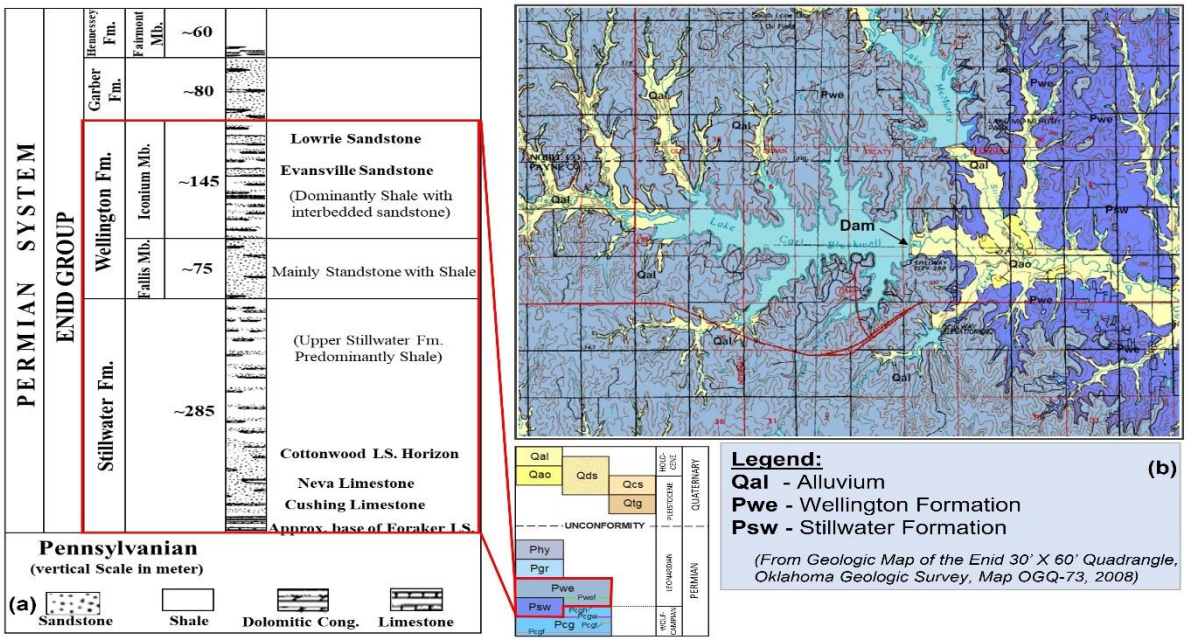

Figure 3.2. a) Modified stratigraphic column showing Permian age deposition within the study area (Petterson, 1933), b) A map showing surficial depositional unit of Quaternary alluvium and Permian bedrock unit of Wellington and Stillwater Formation in the area of Carl Blackwell Lake (Stanley et al., 2008).

The Amec Foster Wheeler Environment & Infrastructure, Inc. conducted a geotechnical study on the Carl Blackwell dam in 2014 and generated a geotechnical report titled Amec Report in 2015 that included information about four boreholes drilled through the dam. The four boreholes (BH1, BH2 BH3, BH4) were drilled at depths ranging from 17 - 37 m down the crest of the dam (Fig. 3.3). All the four-borings show nearly 0.3 – 0.5 m thick soil and vegetation, which is considered the topsoil unit. The embankment fill unit underlies the topsoil unit and consists of stiff to hard clay with different rock fragments and sand in BH1 and BH2, and sandy clay with silty sand in BH3 and BH4 (Fig. 3.3a). The thickness of the dam fill unit ranges between 5 to 20 m, as encountered in BH1 and BH3, respectively. The foundation soil underlying the dam fill unit is alluvium deposits consisting of clay and silt with varying amount of sand that generally increases with depth. The clay and silt within the alluvium soil are mostly medium stiff-to-stiff with the occasional presence of soft to very soft zones (Amec Report, 2015). The thickness of the alluvium varies between 10 m and 20 m, as shown in BH1 and BH4 (Fig. 3.3). The driller reported a very hard clay below the alluvium, causing boring refusals at 37 m depth in BH4 (Amec Report, 2015). This very hard clay is most likely the Wellington Formation shale. A 2-D schematic cross-section A-A' (Fig. 3.3b) was generated based on the borehole information to better comprehend the overall dam structure and the depth of the foundation rock. The cross-section shows that the dam fill unit is thicker (up to a depth of 35 m) at the southern side compared to the northern side. The alluvium unit underlying the dam fill unit shows an average thickness of 20 m with interbedded sandy silt and clay. The bedrock unit lies at a much greater depth (~35 m) at the

southern part of the section and becomes shallower (~20 m) at the northern part of the section.

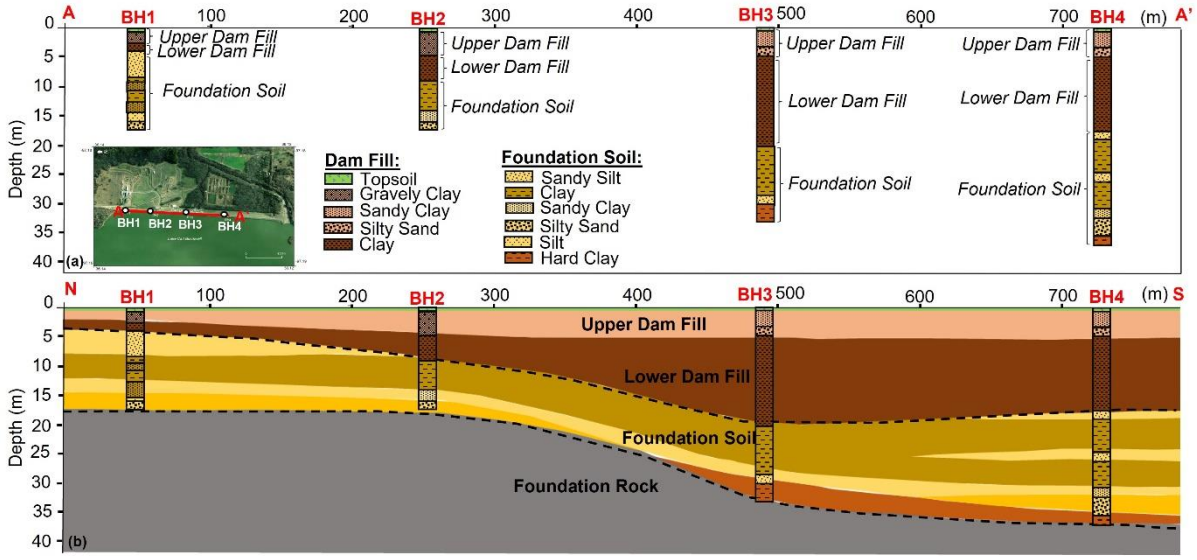

Figure 3.3(a) Location of available boreholes along the dam with their lithological description, and (b) the 2-D schematic cross-section A-A' generated using the borehole information.

3.4 Data Acquisition

Geophysical profiles, including seismic P- wave and S- wave reflections and ERT were collocated all along a 770 m stretch of the dam's crest (Fig. 3.4). The ERT profile was acquired using the 10-channel multi-electrode resistivity meter Syscal Pro having 72 electrodes spaced at 5 m apart and the dipole-dipole electrode configuration in a roll-along sequence. This electrode configuration was adopted because it incorporates stable signal strength of relatively high resolution and reasonable depth of penetration (Nthaba et al.,

2020; Cardarelli et al., 2014; Stummer et al., 2004). The reflection profiles were acquired using the seismic land streamer systems. The data acquisition constraints for both reflection profiles are displayed in Table 1.

Figure 3.4 Map showing the location of the collocated geophysical lines acquired along the crest of the Carl Blackwell dam. The red line marks the location of the geophysical profiles, and BH denotes the borehole locations.

Multichannel analysis of the Love Waves (MALW) signals in the acquired S-wave reflection data generated a two-dimensional S- wave velocity (Vs) profile along the S- wave reflection line. The acquired P-wave reflection data were analyzed to produce a P-wave velocity (Vp) profile all along the reflection profile.

Table 1: Acquisition constraints of P-wave and S-wave reflection profiles.

Acquisition	S-wave Reflection	P-wave Reflection
Recording Channel	24	24
Geophone type	14-Hz Horizontally	40-Hz Vertically
Source type	Rolling source	10-kg Sledgehammer
Geophone interval	0.75 m	2 m
Source interval	1.5 m	2 m
Nominal offset	0.75 m	2 m
Number of stacks	3	3
Sampling rate	1.0 ms	0.5 ms
Recording length	1.0 s	0.5 s
Recording system	Geode	Geode
Field filters	None	None

3.5 Data processing

The processing steps applied to P-wave and S-wave reflection data are reviewed in Figure 3.5. The acquisition geometry was applied to the shot gathers file header for both sources and receivers. A trapezoid bandpass filter was employed to eliminate the low-frequency noises and enhance the P-wave and S-wave signals. A simple application of automatic gain control (AGC) window (100 ms) was applied to reduce the amplitude contrast of the traces, which increased the ratio of signal-to-noise. The surface wave noise attenuation (SWNA) module was used to decrease the influence of ground rolls from the P-wave and Love wave from S-wave data. F-K filtering was used to eliminate the effect of the

remaining ground roll and enhance the reflection signals. A predictive deconvolution module was applied with an operator length and predictive distance of 10 and 20, respectively, to remove multiples from the data and enhance the temporal resolution. The velocity analysis of the processed P- and S-wave data provided estimated stacking velocity fields to stack the data. After stacking the data, frequency-distance (F-X) deconvolution filter of Weiner Levinson type and Trace mixing module was employed to the stacked data to eliminate random noises, enhance lateral continuity of the signal, and balance the trace amplitude laterally. The stacked time profiles were then converted into depth profiles using smoothed stacking velocity fields.

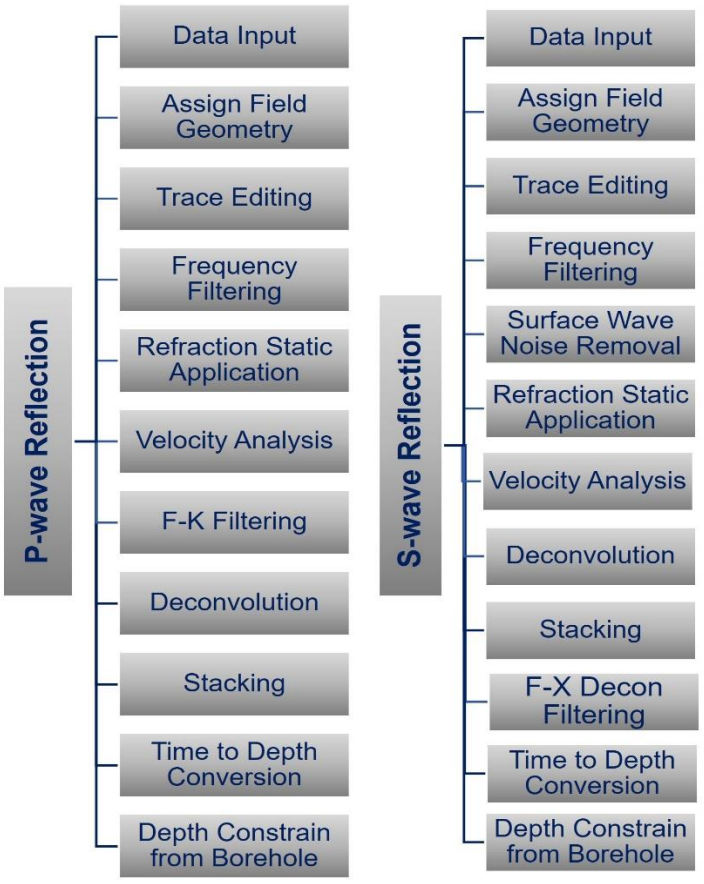

Figure 3.5 The processing steps of P- (left) and S-wave data (right).

The S-wave reflection was processed as MALW data using SurfSeis V6 software (Kansas Geological Survey 2017). The basic steps related in the processing and inversion of MALW data comprise converting the data shot gather from time to frequency domain by Fast Fourier Transform, generation of dispersion curves from the field-based record, obtaining a 1D S- wave velocity (Vs) profile out of the dispersion curves inversion applying an iterative inversion procedure (Fig. 3.6). A least-square method automated the inversion process to calculate the Vs profile (Xia et al., 1999). Only the Vs are updated after every iteration during the inversion process, while other parameters such as Poisson's ratio, model thickness, and density remain unaffected (Park et al.,1999). The inverted 1D profiles are interpolated to generate the 2D subsurface Vs model.

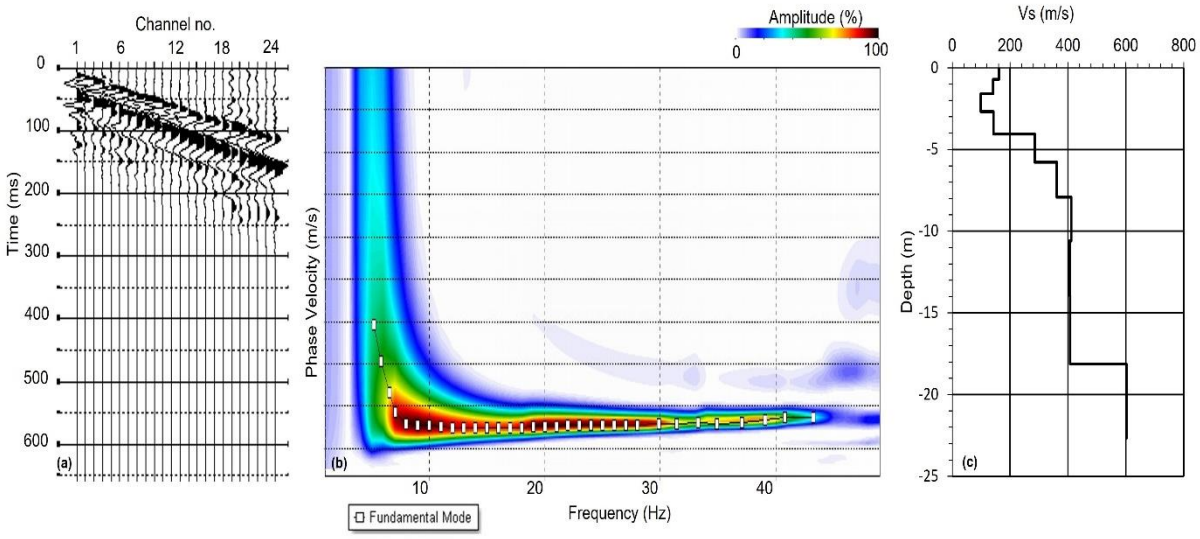

Figure 3.6 The processing procedure for MALW data involving three steps: a) Acquiring time-domain Love wave data (left panel), b) transforming the time-domain gather to frequency-phase velocity domain and picking of dispersion curve (middle panel), and c) Dispersion curve inversion to generate one dimensional velocity-depth profile (right panel).

The first arrivals of the acquired P-wave reflection data were picked and analyzed as seismic refraction data using the SeisImager software (Geometrics, 2009). This software uses a nonlinear least-squares method to invert the travel time. Two types of inversion were carried out in this study, including time-term and tomographic inversion. In the time-term approach, linear least squares are combined with the analysis of delay time for the inversion of first arrivals to generate a velocity section. The time-term inversion process allows generating the Vp of the subsurface at each geophone location along the seismic profile. The first arrival times were picked manually, and travel-time graphs were plotted. Thereafter, layers were assigned to the graphs, and time-term inversion were performed. For the tomographic inversion, a preliminary velocity model was created from the time-term inversion, and rays through the model are traced at different iterations to reduce the root mean square (RMS) error among the observed and estimated travel times.

The ERT data were handled and inverted utilizing Res2DInv software using nonlinear optimization inversion technique (Loke, 2000) to determine the amount of resistivity dispersed within the subsurface. During the inversion, the least-squares inversion technique was used and selected standard least-squares constraints. This method minimized the variation between the calculated and observed apparent resistivity, which indicates more robust inversion results. Appropriate damping factors, number of iterations, and other factors were selected based on the estimated noise amount in the measured records.

3.6 Data Interpretation

The P- wave and S-wave reflection profiles imaged the dam structure, the underlying soil foundation, and the foundation rock (Fig. 3.7). The seismic P-wave reflection profile (Fig. 3.7a) showed three distinct seismic reflectors. The first reflector appeared at 10 m depth below the dam's crest at the northern side of the profile, dipping to 20 m depth towards the south marking the interface among the bottom of the dam fill layer and the top of the alluvium foundation soil (Fig. 3.7a). The foundation soil showed variable thickness increasing from 5 m at the north part to 20 m at the south part of the profile (Fig. 3.7a). The second seismic reflector, which is a relatively strong and coherent reflector, marks the top of the foundation rock layer. This top of the interpreted foundation rock layer appeared at 10 m depth below the dam crest at the northern part of the P-wave profile and showed a gentle southward dip. At a distance mark of 450 m, the depth to the bedrock increased significantly, showing a bedrock depression that extends to the profile's southern part (Fig. 3.7a). This bedrock depression is interpreted as a bedrock valley that has completely eroded the upper bedrock layer or foundation rock down to the second bedrock layer. The third seismic reflector marks the top of a second bedrock layer that appeared at 25 m depth at the northern part sloping southward to reach a 40 m depth at the southern part the profile (Fig. 3.7a).

The S-wave reflection profile (Fig. 3.7b) is relatively of a lower quality compared to the P-wave reflection profile (Fig. 3.7a). This was mainly due to the poor coupling of the shear-wave geophones with the ground surface of the grassy surface of the crest of the dam. Three main seismic reflectors were identified along the S-wave profile, which correlates to those

identified along the P-wave profile. These reflectors delineated the dam fill, foundation soil, and foundation rock. The S-wave reflection profile showed a relatively shallow reflector that characterized the dam fill layer into two main units; the upper dam fill and the lower dam fill (Fig. 3.7b). The upper dam fill thickness varies from 5 to 7 m, and the lower dam fill thickness ranges from 5 to 10 m (Fig. 3.7b).

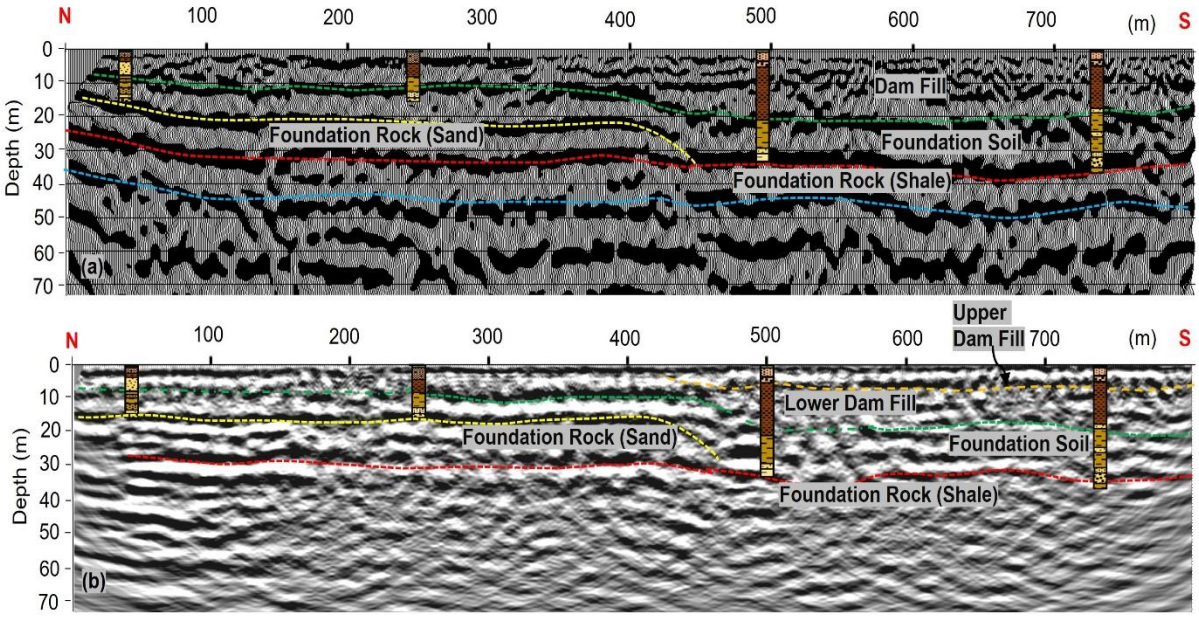

Figure 3.7 a) The Interpreted P-wave (top panel), and interpreted S-wave reflection profile (bottom panel).

The MALW profile (Fig. 3.8a) shows the Vs distribution within the upper 15 m of the body of the dam, delineating three Vs layers along the profile. The first layer (5-7 m thick) has a Vs ranging from 120 to 220 m/s and it corresponds to the interpreted upper dam fill delineated by the S-wave reflection profile. The second layer shows Vs values ranging between 260 and 380 m/s, occurring at depths varies from 7 to 15 m. This layer corresponds to the shallow part of the interpreted lower dam fill delineated by the S-wave reflection

profile. The third Vs layer occurs at an average depth of 10 m with Vs varying from 300 - 500 m/s, interpreted as the shallow part of the foundation soil as delineated by both P- and S-wave reflection profiles. A zone of anomalous low Vs is identified within the lower dam fill, and the shallow part of the foundation soil between distance marks 450 and 600 m (indicated by dashed circles on Figure 3.8a). The Vs anomalous zone is centered around the location of a water intake tunnel running across the dam. This anomalous zone may indicate a weakness zone or potential internal erosion surrounding the intake tunnel within the lower dam fill unit. The MALW profile has a limited depth of penetration and did not delineate the image the foundation rock units.

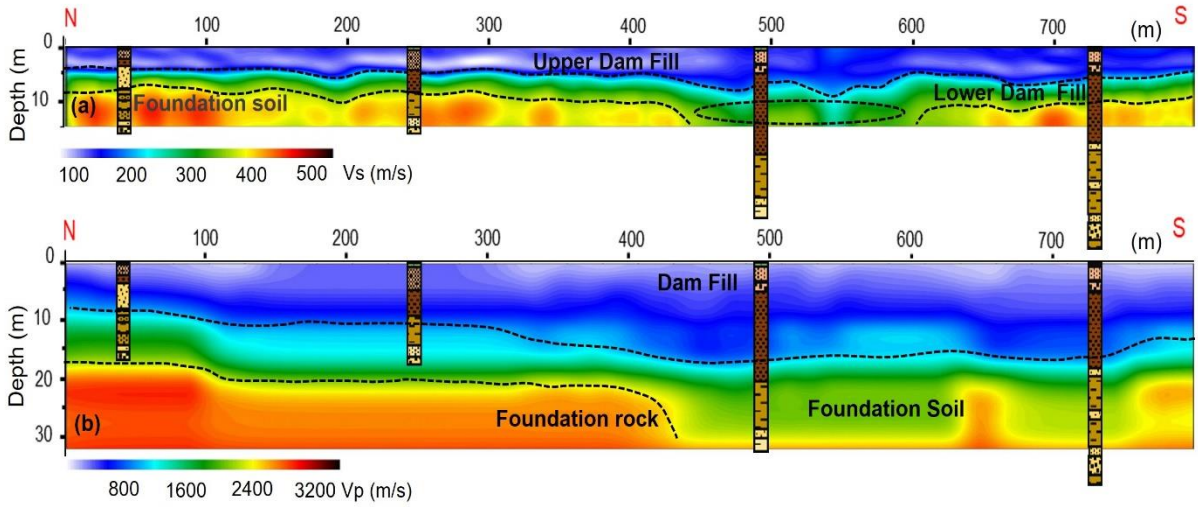

Figure 3.8 MALW profile (a), and P-wave refraction profile (b) along the embankment of the dam

The seismic P-wave refraction profile (Fig. 3.8b) reveals three seismic units. The first unit demonstrates Vp between 500 and 1200 m/s, and a thickness varying from 8 to 15 m,

corresponds to the dam fill materials delineated by the P- wave and S-wave reflection profiles. The second unit exhibits Vp varying from 1250 to 2400 m/s; and corresponds to the foundation soil, as delineated by the P- wave and S-wave reflection profiles. The lateral variation in Vp values within the foundation soil could indicate variation in the degree of compaction. The third seismic unit has Vp ranging from 2450 to 3000 m/s occurring at a depth of 15 m between the northern side of the profile and pinches out at 450 m distance mark, interpreted as the foundation rock (Fig. 3.8b). Same as the seismic P-wave reflection profile, the southern part of the foundation rock seems to have pinched out, marking a bedrock depression or what is interpreted as a bedrock valley.

The ERT profile characterized the body of the dam into five resistivity layers (Fig. 3.9). From upper to lower, the first unit shows relatively high resistivity values (16 to 80 Ωm) increasing southward, interpreted as the upper dam fill. This layer's high resistivity indicates lower moisture content as the water level was lower in the lake (reservoir) than the base of this unit during the resistivity survey. The thickness of this layer increases from 4 m towards the northern side of the profile to 6 m towards the southern side (Fig. 3.9). The second resistivity unit is described by a moderate resistivity (10 to 25 Ωm) with increases in thickness from 5 m at the north part of the profile to 10 m at the south part (Fig. 3.9). This layer corresponds to the lower dam fill, which is mainly clay materials. The resistivity of this layer decreases southward, showing an anomalously low resistivity zone between distance marks 470 and 650 m. Such a low resistivity zone may be caused by higher moisture content and can be a zone of potential seepage or internal erosion. The very low resistivity zone at a distance mark between 550 – 600 m within this layer may be referred to the materials

around the water intake tunnel across the dam. The third resistivity layer is characterized by moderate ranges of resistivity values from 15 - 30 Ωm, inferred as the dam foundation soil. The thickness of this layer increases from a lowest of 5 m along the northern part of the ERT profile to a highest limit of 15 m corresponding to the bedrock valley fill in the southern side of the profile.

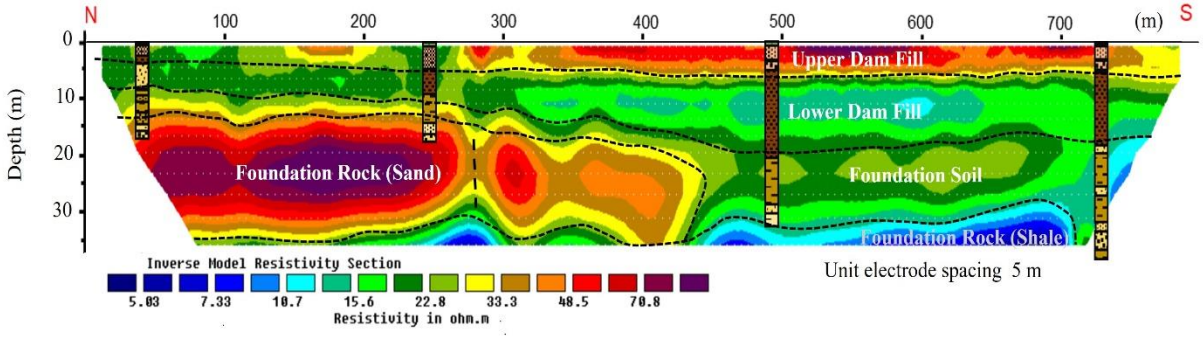

Figure 3.9: The resistivity profile along the crest of the dam annotated with interpretations.

A fourth resistivity layer shows resistivity values with high ranges (30 to 80 Ωm), extending from the most northern side of the profile and pinches out at a distance mark 450 m (Fig. 3.9). This layer is interpreted as the foundation rock, which is most likely the Wellington Sandstone Formation. After distance mark 450 m of the profile, the interpreted Wellington Sandstone Formation seemed to be completely eroded down to Wellington Shale Formation. A relatively lower resistivity plane (marked by a dashed black vertical line) was observed at a distance mark 280 m within the sandstone bedrock where a water intake structure of USDA is located. This linear feature could indicate a plane of weakness/fracture within the bedrock at this location. The fifth resistivity layer shows significantly low

resistivity (<10 Ωm) along the length of the ERT profile (Fig. 3.9), interpreted as the Wellington Shale Formation delineated by both P- and S-wave reflection profiles.

3.7 Discussion

The integration of multiple geophysical methods, including seismic P- and S-wave reflection, ERT, MALW, P-wave refraction, and borehole information along the embankment of the Carl Blackwell dam has provided better characterization of the dam. The geophysical surveys characterized the dam fill (upper and lower fill), the foundation soil, and the layered foundation rock units. Overlaying the ERT profile on the collocated P-wave reflection profile (Fig. 3.10a) is a good example of how the integration of electrical and seismic profiling can improve the subsurface characterization.

All geophysical surveys revealed that the dam fill unit (5 to 15 m thick) showed lateral variability and was characterized into upper and lower dam fill units. The upper dam fill unit (5-7 m thick) made of coarse to medium grain silty sand or sandy clay with occasional rock fragments was characterized by high resistivity, low Vs, and low Vp. These characteristics indicate that the unit has low moisture content and less compaction. The lower dam fill (4 to 15 m thick), mainly clay materials, was characterized by higher Vs compared to the upper dam fill, moderate resistivity, and low Vp. The resistivity of the lower dam fill decreased southward, showing a zone of anomalously low resistivity among the distance marks 500 and 650 m. The overlay of the MALW interpretation on the top of the collocated ERT profile indicates that the low resistivity zone corresponds to the low Vs zone within the lower dam

fill (marked by red dashed circle in figure 3.10b). The center of the anomalous area identifies the location of a water intake tunnel running across the dam at this location. This anomalous zone may indicate higher moisture content and could be a zone of potential seepage or internal erosion within the materials surrounding the water intake tunnel in the lower dam fill unit.

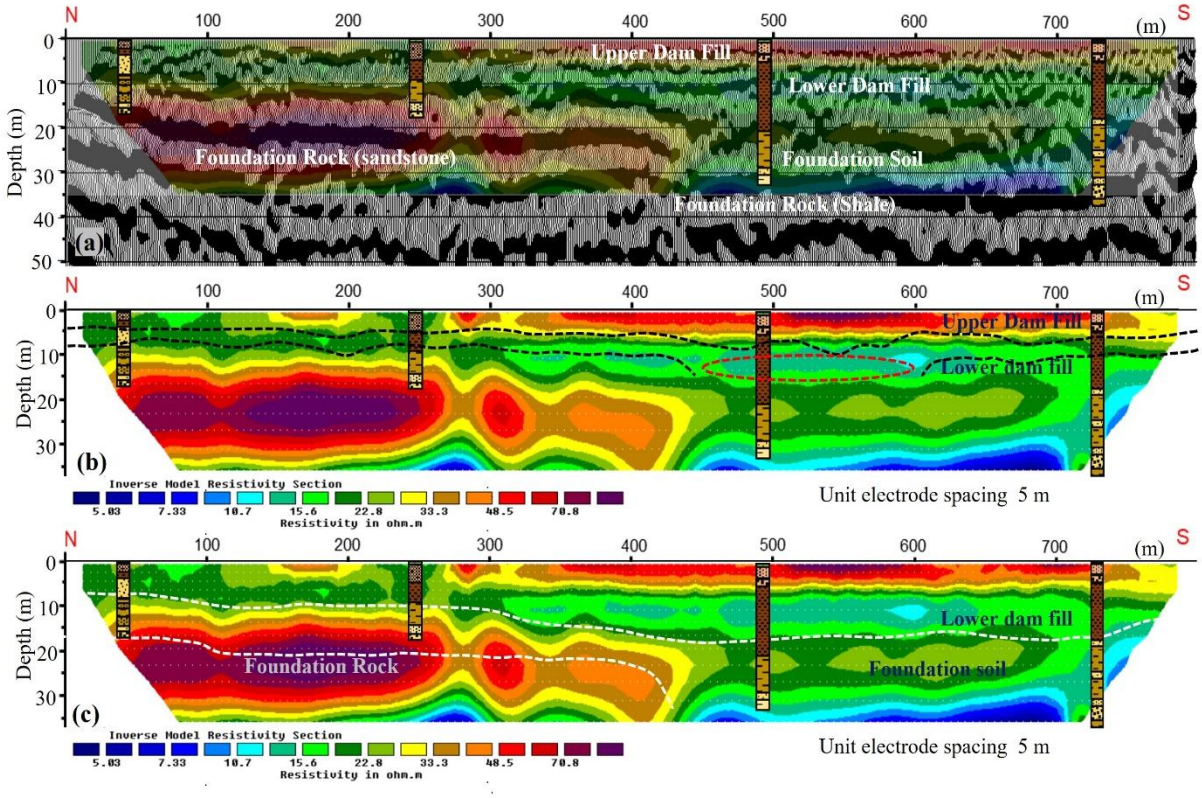

Figure 3.10: a) The ERT profile superimposed on the collocated P-wave reflection profile, b) The interpretation of the MALW profile (black dashed lines) superimposed on the collocated ERT profile, and c) The interpretation of the refraction profile (white dashed lines) superimposed on the collocated ERT profile.

The foundation soil (8-20 m thick), composed of alluvium, was well delineated by the ERT and refraction profiles (Fig. 3.10c). The MALW profile imaged only the upper part of the

soil foundation. The soil foundation was interpreted by moderate Vs, Vp, and resistivity values, indicating that this unit is less likely to have seepage zones or internal erosion. The underlying foundation rock of the dam was well imaged by the P-wave and S-wave reflection, P-wave refraction, and ERT profile. The top of the foundation rock showed a gentle dip southward and a bedrock depression between the distance mark 450 m and the most southern part of the surveyed profile. The high resistivity of the foundation rock indicates that it is most likely made of the Wellington Sandstone, eroded down to the Wellington shale below the interpreted bedrock valley. Nearly 20 m thick alluvium sediments filled the bedrock valley. A linear and vertical fracture within the sandstone foundation rock at a distance mark 280 m where the USDA water structure is located along the ERT profile could be a possible pathway for groundwater seepage through the sandstone foundation rock. This feature may need to be further investigated with different ERT configuration combined with other methods to determine whether it is real and can pose a risk on the safety of the foundation rock of the dam or it is inversion artifacts. The shale bedrock layer showed under the interpreted bedrock valley seemed to extend along the length of the surveyed profiles with a gentle southward slope.

Despite the usefulness of integrating multiple geophysical methods for characterizing the dam body and its underlying foundations, some of the methods were more effective than others. While the P-wave seismic reflection has successfully imaged multiple bedrock layers below the dam, the method lacked the vertical resolution to characterize the dam fill units. The S-wave reflection method showed a better vertical resolution and characterized the dam fill into upper and lower units. However, data quality remained poor due to a lack of

better coupling between the S-wave geophones of the land streamer and the ground surface. Data acquisition needs to be conducted using conventional spiking geophones. The MALW profile generated from the acquired S-wave reflection data was of a very limited depth. A separate survey to acquire surface wave data using a more extended geophone array and a heavier source is deemed necessary to image the dam and the underlying foundations.

3.8 Conclusion

This study investigated the combination of multiple geophysical techniques and borehole data to characterize the embankments of an earth-fill dam and underlying foundations. The results of all the geophysical methods (P- and S-wave reflection, ERT, P-wave refraction, and MALW) and the available borehole data showed good agreement. They revealed the detailed dam geometry, the foundation soil, and the foundation rock. The embankment of the dam has been characterized into dam fill (upper and lower unit), foundation soil, and layered foundation rock. The low resistivity, low Vs, and low Vp within the dam fill may indicate possible potential seepage or internal erosion. All geophysical surveys have detected variations in the depth to the foundation rock and its lateral variations, except the MALW profile that was limited to a shallow depth. The southern part of the Sandstone foundation rock appeared to have been eroded away and later filled with alluvium deposits forming a 20 m thick bedrock valley. The underlying shale foundation rock appeared to be relatively flat with a gentle southward slope. This study showed that

geophysical methods could be utilized to assess and improve dams' safety non-invasively and at a relatively cheaper cost. The study also demonstrated the efficacy of integrating seismic and electrical resistivity methods for a better characterization of the dam and provided insights on how to optimize the survey designs to provide optimum results to investigate dams.

References

Abdulsamad, F., Revil, A., Ahmed A.S., Coperey, A., Karaoulis, M., Nicaise, S., Peyras, L., 2019. Induced polarization tomography applied to the detection and the monitoring of leaks in embankments. Engineering Geology 254, 89-101. https://doi.org/10.1016/j.enggeo.2019.04.001

Adams, G. P., Bergman, D. L., 1996. Geohydrology of alluvium and terrace deposits of the Cimarron River from Freedom to Guthrie, Oklahoma. US Department of the Interior, US Geological Survey, Vol. 95, No. 4066.

Avalos, E. B., Malone, D. H., Peterson, E. W., Anderson, W. P., and Gehrels, R. W., 2016. Two-dimensional seismic refraction tomography of a buried bedrock valley at Hallsands beach, Devon, United Kingdom. Environmental Geosciences 23(4), 179-193.

Bond, L.J., Kepler, W.F, Frangopol, D.M., 2000. Improved assessment of mass concrete dams using acoustic travel time tomography: Part I. Theory. Construction and Building Materials 14, 133 – 146.

Cardarelli, E., Cercato, M., and De Donno, G., 2014. Characterization of an earth-filled dam through the combined use of electrical resistivity tomography, P-and SH-wave seismic tomography and surface wave data. Journal of Applied Geophysics 106, 87-95.

Cardarelli, E., Cercato, M., and Di Filippo, G., 2010. Geophysical investigation for the rehabilitation of a flood control embankment. Near Surface Geophysics 8(4), 287-296.

Carnevale, M., Hager, J. L., and Buller, R. A., 2011, January. Investigation of source of seeps beneath earthen dam, Central Massachusetts. In Symposium on the Application of Geophysics to Engineering and Environmental Problems, pp. 379-387. Society of Exploration Geophysicists.

Darold, A. P., Holland, A. A., 2015. Preliminary Oklahoma optimal fault orientations: Oklahoma Geological Survey. Open-File Report OF4-2015.

Dezert, T., Fargier, Y., Lopes, S. P., and Côte, P., 2019. Geophysical and geotechnical methods for fluvial levee investigation: A review. Engineering Geology 260, 105206.

Geometrics Inc., 2009, SeisImager/2D software manual; version 3.3, p. 257. https://geometrics.com/wp-content/uploads/2019/05/SeisImager2D_Manual_v3.3.pdf

Hickey, C. J., Römkens, M. J., Wells, R. R., and Wodajo, L., 2015. Geophysical methods for the assessment of earthen dams. In Advances in Water Resources Engineering, pp. 297-359. Springer, Cham.

Hunter, L. E., Powers, M. H., Haines, S., Asch, T., Burton, B. L., and Crustal Imaging and Characterization Team., 2007, January. Geophysical investigation of the success dam foundation: An Overview. In Symposium on the Application of Geophysics to

Engineering and Environmental Problems, pp. 21-30. Society of Exploration Geophysicists.

Ikard, S. J., Rittgers, J., Revil, A., and Mooney, M. A., 2015. Geophysical investigation of seepage beneath an earthen dam. Groundwater 53(2), 238-250.

Inazaki, T., 2007, April. Integrated geophysical investigation for the vulnerability assessment of earthen levee. In 20th EEGS Symposium on the Application of Geophysics to Engineering and Environmental Problems, pp. cp-179. European Association of Geoscientists & Engineers.

Ismail, A., Abdelnaby, A., Larson, T., 2017. High-resolution P-and S-wave seismic reflection followed by engineering modeling for geotechnical site characterization in Southern Illinois. Journal of Environmental and Engineering Geophysics 22 (4), pp. 375-384. https://doi.org/10.2113/JEEG22.4.375.

Ismail, A., Denny, F. B., and Metwaly, M., 2014. Comparing continuous profiles from MASW and shear-wave reflection seismic methods. Journal of Applied Geophysics 105, 67-77.

Jaiswal, P., Gregg, J. M., Parks, S., Holman, R., Mohammadi, S., and Grammer, G. M., 2019. Evidence of fault–fracture “Hydrothermal” reservoirs in the southern midcontinent Mississippian Carbonates. The American Association of Petroleum Geologists 122. https://doi.org/10.1306/AAPG122

Kansas Geological Survey, Surfseis MASW Software overview. https://www.kgs.ku.edu/software/surfseis/s2intro.html, 2017 (accessed 4th November 2021).

Karastathis V. K., Karmis P.N., Drakatos G., and Stavrakakis G., 2002. Geophysical methods contributing to the testing of concrete dams. Application at the Marathon dam. Journal of Applied Geophysics 50(3), 247-260.

LeBlanc, S. L., 2014. High resolution sequence stratigraphy and reservoir characterization of the" Mississippian Limestone" in north-central Oklahoma. Doctoral dissertation, Oklahoma State University, 9 pp.

Loke, M. H., 2000. Electrical imaging surveys for environmental and engineering studies. A practical guide to 2-d and 3-d surveys, 61.

National Inventory of Dams (NID), Carl Blackwell Dam NID data. https://nid.usace.army.mil/ords/f?p=105:113:5312634610476::NO:113,2:P113_recordid:63472, 2018 (accessed 4th November 2021).

Northcutt, R. A., Campbell, J. A., 1998. Geologic provinces of Oklahoma. In Basement Tectonics 12 (pp. 29-37). Springer, Dordrecht.

Nthaba, B., Shemang, E., Hengari, A., Kgosidintsi, B., and Tsuji, T., 2020. Characterizing coal seams hosted in Mmamabula Coalfield, central Botswana using pseudo-3D electrical resistivity imaging technique. Journal of African Earth Sciences 167, 103866. https://doi.org/10.1016/j.jafrearsci.2020.103866.

Nwokebuihe SC, Alotaibi AM, Elkrry A, Torgashov EV, Anderson NL. 2017. Dam seepage investigation of an Earthfill dam in Warren County, Missouri using geophysical methods.

Oklahoma Water Resources Board (OWRB), Oklahoma lakes report with Beneficial Use Monitoring Program (BUMP). https://www.owrb.ok.gov/quality/monitoring/bump/pdf_bump/Reports/Lakes2017.pdf, 2017 (accessed 4th November 2021).

Park, D., Kishida, T., 2018. Shear wave velocity profiles of fill dams. Soil Dynamics and Earthquake Engineering 104, 250-258.

Park, C. B., Miller, R. D., and Xia, J., 1999. Multichannel analysis of surface waves. Geophysics 64(3), 800-808.

Patterson, J. M., 1933. Permian of Logan and Lincoln counties, Oklahoma. AAPG Bulletin 17(3), 241-256.

Saad, R., Syukri, M., Nordiana, M. M., and Ismail, N. A., 2013. Water table Delineation for Leachate Identification using 2-D Electrical Resistivity Imaging (2-DERI) and Seismic Refraction at Gampong Jawa, Banda Aceh. The Electronic Journal of Geotechnical Engineering 18, 1529-1535.

Sazal, Z., Ismail, A., and Sanuade, O., 2021. Geophysical investigation at Carl Blackwell Dam, Stillwater, Oklahoma. Symposium on the Application of Geophysics to Engineering

and Environmental Problems Proceedings, 88-88. https://doi.org/10.4133/sageep.33-047.

Sjödahl, P., Dahlin, T., Johansson, S., and Loke, M. H., 2008. Resistivity monitoring for leakage and internal erosion detection at Hällby embankment dam. Journal of Applied Geophysics 65(3-4), 155-164.

Stanley, T. M., Miller, G. W., and Standridge, G. R., 2008. Geologic map of the Enid 30 x 60 quadrangle, Garfield, Kingfisher, Logan, Noble, Osage, Pawnee, and Payne Counties, Oklahoma. Oklahoma Geological Survey.

Stare, D. P., Hockenberry, A. N., Dreese, T. L., Wilson, D. B., and Bruce, D. A., 2012. Protection of embankments during drilling and grouting. Grouting and Deep Mixing, 1304-1313.

Stummer, P., Maurer, H., and Green, A.G., 2004. Experimental design: electrical resistivity data sets that provide optimum subsurface information. Geophysics 69, 120–139. https://doi.org/10.1190/1.1649381.

Woolery, E. W., 2018. SH-Mode Seismic-Reflection Imaging of Earthfill Dams. Engineering 4(5), 694-701. https://doi.org/10.1016/j.eng.2018.08.009.

Xia, J., Miller, R. D., and Park, C. B., 1999. Estimation of near-surface shear-wave velocity by inversion of Rayleigh waves. Geophysics 64(3), 691-700.

CHAPTER IV

GEOPHYSICAL INVESTIGATION OF THE EMBANKMENT SECTION OF THE ROBERT S. KERR DAM, LOCUST GROOVE, OKLAHOMA

4.1 Abstract

Robert S. Kerr Dam in Central Oklahoma is a concrete gravity structure with an earth-filled embankment section and a concrete ogee weir spillway. The earth-filled embankment section consists of 20 meters of fill materials on the top of a Mississippian limestone and chert bedrock. Dam's internal erosion, seepage piping, and fracturing in the bedrock pose hazards to the dam's safety and need to be investigated at early stages. In this study, I conducted multiple geophysical surveys along the top and toe of the embankment section of Robert S. Kerr Dam to investigate the earth-filled embankment and the underlying rock foundations. Conducted geophysical surveys, included seismic shear-wave reflection, P-wave refraction, multi-channel analysis of surface wave (MASW), and electrical resistivity tomography (ERT). Results of the geophysical surveys characterized the embankment fill materials into two zones, with the lower zone being probably more compacted. The soil

foundation under the embankment was delineated as a relatively more compacted and homogenous unit. The rock foundations (bedrock) were characterized into two units; an upper unit with an average thickness of 20 m interpreted as limestone and chert of the Reed Spring Formation and a lower unit interpreted as the Chattanooga shale Formation. Below the most northern part of the embankment, the bedrock showed a 6 m vertical displacement, probably due to erosion or a structural feature. Local geophysical anomalies in the upper bedrock were interpreted as potentially fractured zones. This study showed that integrating multiple geophysical methods has successfully characterized the embankment and the underlying rock foundation. Comparing the geophysical results from Robert S. Kerr Dam and the Carl Blackwell Dam in chapter III indicates that the surface conditions and the nature of the rock foundations at the surveyed dams significantly control the efficacy of the applied geophysical surveys. The study also improves our understanding of the advantages and limitations of the geophysical methods applied for earth-fill dam investigations.

4.2 Introduction

Dams are engineering structures that play significant roles in power generation, water storage, flood control, recreational, and eco-system management (Hickey et al., 2015). Dams are often susceptible to internal erosion, seepage and piping, and fracturing which can ultimately take the lead to potential dam failure (Omofunmi et al., 2017; Zhang and Chen, 2006; Fell et al., 2003). Hence, these structures require routine monitoring and evaluation of the condition of their foundation and internal body to avoid potential hazard. Aging is another concerning factor that could lead to potential dam failure (Nwokebuihe et al., 2017). While the safety of 95% of nation's dams are maintained by the state and local authorities,

there are many older dams lacked the needed maintenance to guarantee the operational integrity posing potential failure hazard to the downstream population (Lane, 2007).

Robert S. Kerr Dam is a concrete gravity structure with an earth-filled embankment section. The dam has history of potential seepage through the right (north) abutment near the embankment area and has been classified as Potential Failure Mode (PFM) category II (GRDA, 2012). Seepage can be a serious maintenance issue which can extremely degrade the stability of the dam structure over time. More so, the dam has exceeded the economic lifetime of 50 years suggested by the Soil Conservation Service (SCS) (Hickey et al., 2015). Thus, it has been classified as a high hazard potential yield dam based on the assessment of expected impact upon potential failure (NID, 2021). It is essential to investigate the dam's structural integrity and its underlying foundation to supplement the existing monitoring program as well as routinely inspect the dam as a part of the risk reduction action to locate any potential seepage and material transport path for the future. Considering the possible risk, the failure of the dam could pose to the environment, rapidly functioning and cost-effective methods are required to identify and routinely monitor the heterogeneous or anomalous weak zones and assess geotechnical condition of the dam (Bievre et al., 2017).

Geophysical methods measure a set of parameters which are associated to numerous physical properties of the subsurface materials and their spatial distribution (Putiška et al., 2012; Chalikakis et al., 2011; Jongmans and Garambois, 2007). These methods have extensively gained attention to assess the geotechnical conditions of dams due to their technological advancement over past decades. Amongst these geophysical techniques, the

electrical resistivity is the extensively used technique for dam investigation to detect zones of fissuring, fractures, desiccation cracks, and seepage forming in the embankment or dam structure (Jones et al., 2014; Lin et al., 2013). Fracture zones are often characterized by low resistivity anomaly associated with high water saturation, clay or the presence of weathered material. Although this method is fast, it is often sensitive to moisture or clay content that change with time, therefore this method is non-unique and requires integration with other techniques (Cardarelli et al., 2014; Ikard et al., 2015; Telford et al., 1990).

Recently, seismic methods have gained much attention in the characterization of earth fill dam embankment (Bievre et al., 2017). For instance, Seismic P-wave refraction has been employed to locate low velocity zones for non-saturated earth dam and determine the depth of the bedrock (Cardarelli et al., 2010). Seismic shear (S)-wave reflection method has been employed to image earth fill dam foundation and internal structure of a dam for remedial engineering in a cost-effective manner (Woolery, 2018). This method demonstrated success in distinguishing in-situ geologic deposits and dense engineered borrow-fill of comparable substance by depicting low-contrast intra-embankment limits (Woolery, 2018). In addition, the inversion of surface waves has been used for characterization of internal structure of the dam body (Cardarelli et al., 2014; Cardarelli et al., 2010). The seismic shear wave velocities (Vs) from the Multichannel Analysis of Surface Waves (MASW) were applied to characterize the shear strength (young's modulus and dynamic shear) and compactness of the levee and embankment materials (Morris, 2012; Karl et al., 2011).

Geophysical techniques are rapid, cost-effective, and non-invasive, making them advantageous for investigating sensitive structures like dams and embankments. However, they are non-unique and often require additional data for accurate interpretation. Near surface conditions and inherent time-varying properties in the subsurface are often specific to the investigation site and have significant effect on the quality of the results of the geophysical methods (Baker et al., 2002). For the seismic S-wave reflection method, an excellent source and geophone coupling to the ground is very crucial as the relative amplitude of the reflection is a function of the geophone coupling in the ground (Steeples and Miller, 1998). The signal quality can be greatly compromised by poor source and geophone coupling to the ground enhancing the ground roll. Integrating multiple geophysical techniques and constraining the geophysical interpretation with known geologic conditions, such as borehole information, can be an efficient practice to overcome the non-uniqueness issue of the geophysical methods.

In this research, a suite of geophysical surveys including Seismic S-wave reflection, electrical resistivity tomography (ERT), MASW, and seismic refraction techniques to depict the embankment section of the Kerr dam and its underlying bedrock with the aim of inspecting the dam for internal erosion, any zone of weakness/seepage in the body or its underlying foundation. The result of this geophysical study will provide information to provide better understanding of the embankment and areas around the downstream and provide methods for temporal monitoring for the entire dam structure and its underlying foundation conditions. This study also contributes to the knowledge of applicability of different geophysical methods based on the near surface conditions of the investigation site.

4.3 Site Description and Geology

Robert S. Kerr dam is located around 15 km southeast of the Pryor, Oklahoma and 4 km north- northwest (NNW) of Locust Grove, Oklahoma (Fig. 4.1a) and is controlled by the Grand River Dam Authority (GRDA). The dam was built in 1964 across the Grand (Neosho) river holding the Lake Hudson with maximum storage capacity of 697,747,565.5 cubic meter and maximum discharge rate of 20,841.2 cubic meter per second (NID, 2021). The dam consists of two main components: a concrete gravity section at the south abutment and an earthen fill embankment section at the north abutment (Fig. 4.1b). The concrete portion is a composite structure which is nearly 425 m long including a powerhouse with four hydroelectric generating units, the ogee spillway, and two non-overflow transition sections (GRDA, 2012). The earthen fill embankment portion is approximately 720 m long with upstream and downstream slope of 3H:1V and 2.5H:1V (horizontal and vertical ratio), respectively. The elevation of the crest of the embankment is 196 m with a width of 9 m. This embankment extends to the north abutment and wraps around the north transition monolith (GRDA report, 2012). An access road passed through the crest of the embankment up to the spillway of the dam. The upstream part of the embankment is wrapped by 1 m thick ripraps up to the crest with a 3 m wide at elevation of 186 m. The downstream side is covered with vegetation up to the crest having ripraps up to a similar bench at an elevation of 188 m.

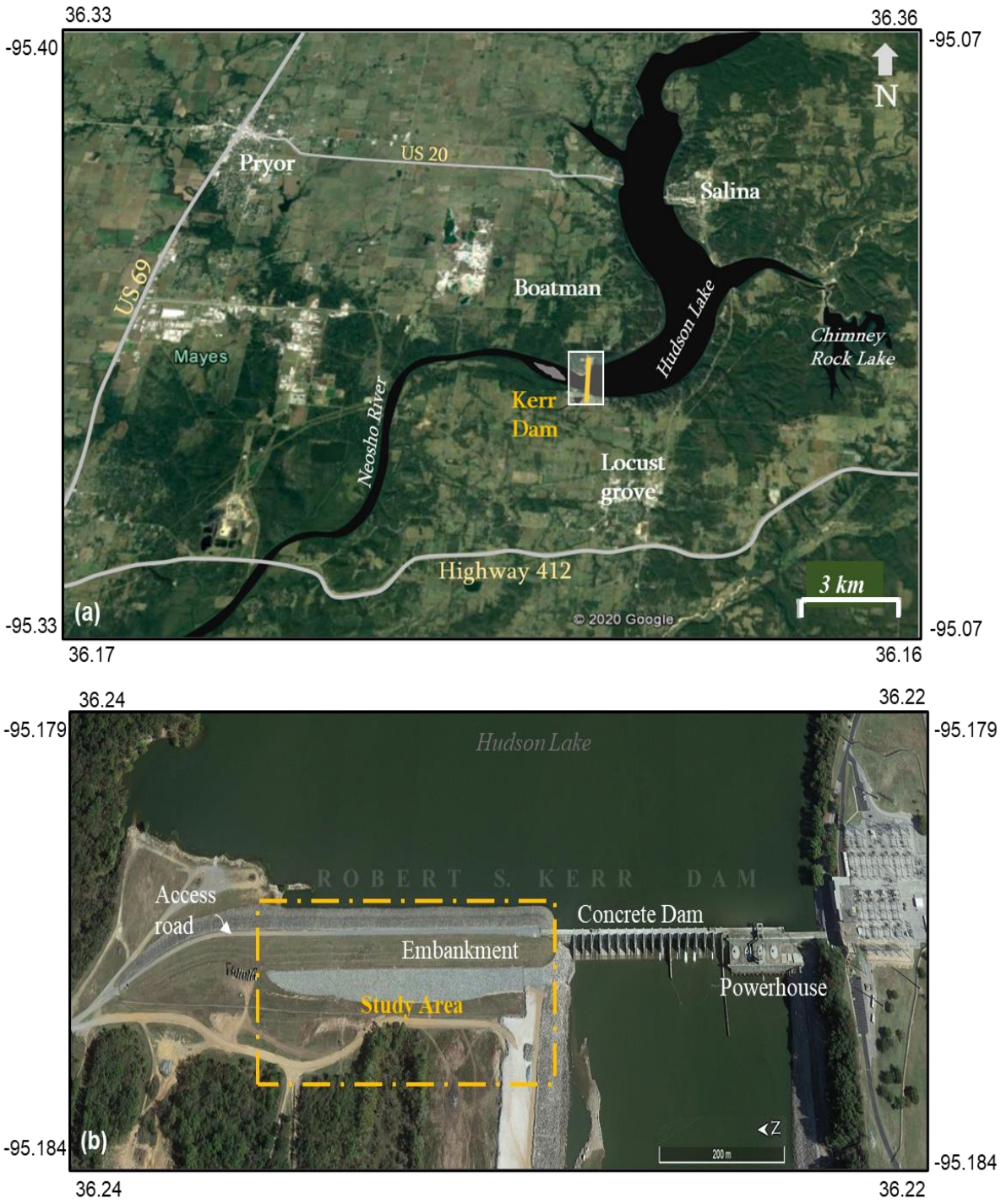

Figure 4.1: Map showing the location of the Kerr dam (a), and the major component of the dam with the study area (b).

Robert S. Kerr dam is located within the vicinity of a geological structure known as the Ozark Uplift (Huffman, 1960). This structure comprises of a major part of the northeastern Oklahoma, northern Arkansas, and southern Missouri. The axis of the structure trends northeast-southwest plunging southwestward into northeast Oklahoma. It is an asymmetric dome shaped broad structure which is segregated into three major Provinces: Springfield Structural plain, Boston Mountain, and Salem Platform (Huffman, 1960). The study area is located within the Springfield Structural plain, which comprises the northern, western, and southcentral part of the uplift and underlain by mostly Mississippian aged rock units. There are two major regional faults identified within the vicinity of the area (Osborn, 2001). A southwest-northeast trending Seneca Fault which is nearly 160 km long located 11 km northwest of the dam, and a north-northeast trending Locust Grove Fault which is nearly 18 km long located 4 km southeast of the Kerr dam (Fig 4.2). Locally, two small high-angle shears were noted along the west side of the powerhouse access road about 800 m south of the powerhouse. However, no other evidence of local shears or faults was found in drill cores from the study location.

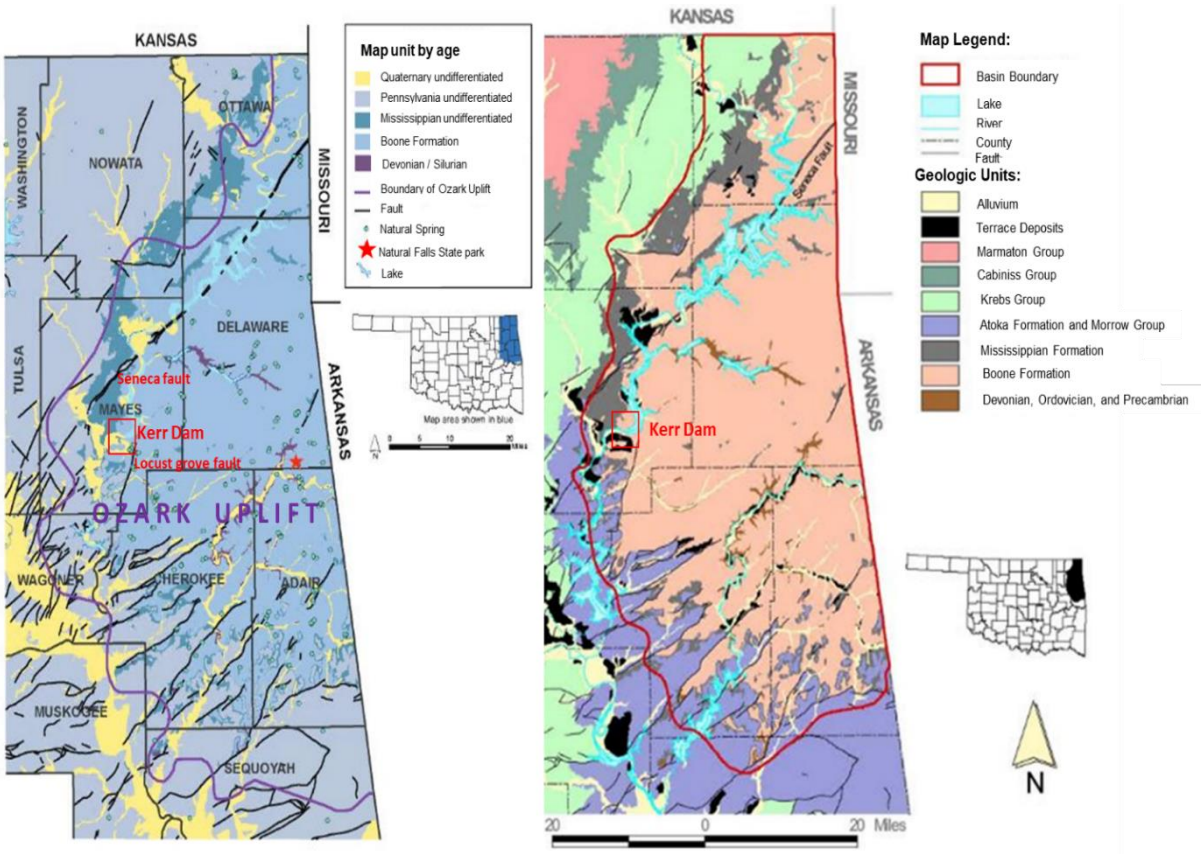

Figure 4.2: Map of the Ozark uplift area showing the major faults (Seneca and Locust Grove) in the surrounding of the study region (Osborn, 2001) (left). Map displaying the dissemination of the geological units within the Ozark uplift area (revised from Cederstrand, 1997) (right).

The dam is underlain by the quaternary alluvium deposits that covers the Mississippian-age bedrock. The quaternary deposits are characterized by loosely consolidated alluvium sediments deposited along the valley floor of all the major streams and many tributaries. Local terrace deposits all along the Grand River surrounding of the town Locust Grove were deposited which is characterized by sand, silt, and chert gravel (Huffman, 1960). The Bedrock consist of the Keokuk, Reeds Spring Formations, and the underlying St. Joe Group. The Keokuk formation consist of white to gray mottled fossiliferous chert locally interbedded

with irregular springers of bluish gray, dense, fine-grained limestone and greenish to black shales in the topmost units (Mazzullo et al. 2013; Choquette et al. 1992; Huffman et al. 1966). The lowermost beds consist of cherty crinoidal carbonate rock (Fay and Friedman, 1979). This unit is highly fractured and weathered as tripolitic chert. Keokuk Formation unconformably overlies the Reeds Spring Formation, which is characterized by alternating equal amount of thin, fine-grained, dense, thinly bedded limestone and dark gray to bluish gray chert (Huffman et al., 1966). This unit is greatly distributed in the northeastern Oklahoma and exposed where the overlying highly fractured Keokuk Formation eroded by deep stream cut. Reeds Spring Formation unconformably overlain the St. Joe Group which is widely distributed over the northeastern Oklahoma through discontinuous outcrop. This unit is characterized by gray thickly bedded crystalline limestone with olive green, soft, limy shale.

4.4 Data Acquisition

Geophysical surveys including S-wave reflection, MASW, ERT, and P-wave refraction were collocated along the top and the bottom of the embankment (Fig. 4.3a). The S-wave reflection profiles were obtained employing seismic land streamer technique. The length of each profile is 450 m long ended up to the concrete part of the dam. The data were collected using 24 horizontally polarized 14 Hz geophones positioned at a spacing of 0.75 m with 0.5 ms of sampling rate. S-wave energy was created with impact of a 3 kg sledgehammer striking horizontally on a cylindrical metal roller source as described by Sazal et al., 2021. Three shots were assembled for every shot location to enhance the signal to noise proportion keeping

the shot interval of 1.5 m. Data were documented with the Geode recoding system with 0.5 s of record length.

The MASW profile of 450 m length was acquired using a surface wave land streamer system using 24 vertical 4.5 Hz geophones positioned at 1.5 m spacing with a sampling rate of 1.0 ms. Surface wave energy was produced using a 10 kg sledgehammer impacted vertically on a flat metal slab positioned on the ground. Shots were stacked three times at each shot locations keeping a source interval at 9 m. The data recording length was 1.0 s using the Geode recording system. Acquired data were processed to create S-wave velocity (Vs) – depth profile.

ERT profiles were acquired along 255 m transects at the top and bottom of the embankment using Syscal Pro resistivity meter of a 10-channels with 52 electrodes. The electrode configuration of dipole-dipole was used with 5 m electrode spacing. Surface wave land streamer data were analyzed to generate a P-wave refraction velocity (Vp) profile.

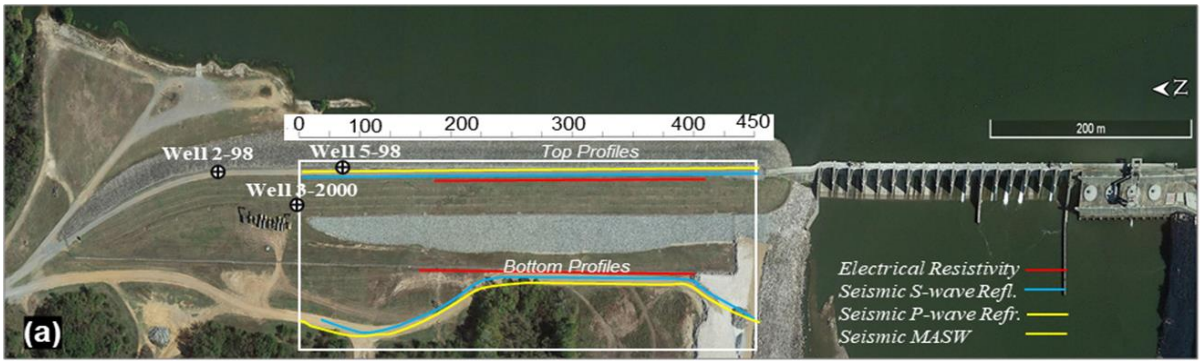

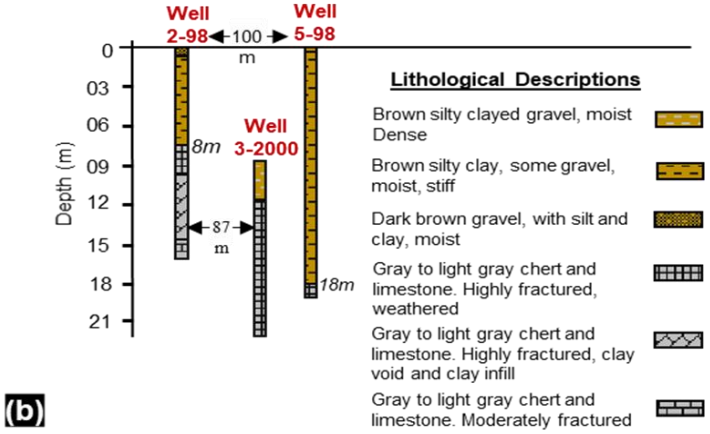

Acquired Geophysical Data from the Kerr Dam site		
Data type	**Number of Lines**	**Line Length**
Seismic S-wave reflection	2	450 m
MASW	2	450 m
Electrical Resistivity	2	255 m
Seismic P-wave refraction	2	450 m

Figure 4.3: Location map of the acquired geophysical data at Kerr dam (a), and locations and description of existing wells (b).

4.5 Data Processing

The acquired S-wave data were processed employing Landmark ProMax software. A simple processing scheme was used to the data following the processing conceptions of Hunter et al. (1984), Miller (1992) and Yilmaz (2001). A very cautious top mute of the direct and refracted arrivals was employed to prevent interpretation of these arrivals as coherent reflector (Steeples and Miller, 1998). A combination of top mute, bandpass filtering and f-k filtering was efficient in subduing the noise in the data triggered by high-frequency airwaves

and low-frequency ground roll (Stumpf and Ismail, 2013). A time-varying spectral analysis, velocity analysis, normal move-out correction (NMO), elevation static correction, and stacking were also performed.

The ERT data were processed employing the RES2DINV software using the finite element approach (Loke and Barker, 1996). This technique is attributed to determine the amount of resistivity dispersed within the subsurface (Loke, 2000). The apparent resistivity distribution (2D pseudo-segments) was produced using the measured resistance along each profile. These pseudo-segments were inverted in 2D using RES2DINV. A finite element model of the resistivity dispersion in the subsurface was created for this inversion to minimize the difference between model response and the calculated data (Sjödahl et al., 2005).

The acquired MASW was processed and inverted using SurfSeis V6 software (Kansas Geological Survey 2017). The software uses Fast Fourier Transformation, to convert the data as of time to frequency domain. Then a dispersion curve was generated from the field record and a 1D S-wave velocity (Vs) profile was obtained from this dispersion curve applying an iterative inversion method. The Vs profile was calculated using a least-square method which automated the inversion process. 2D subsurface Vs model was interpolated from the inverted 1D profiles (fig. 4.4).

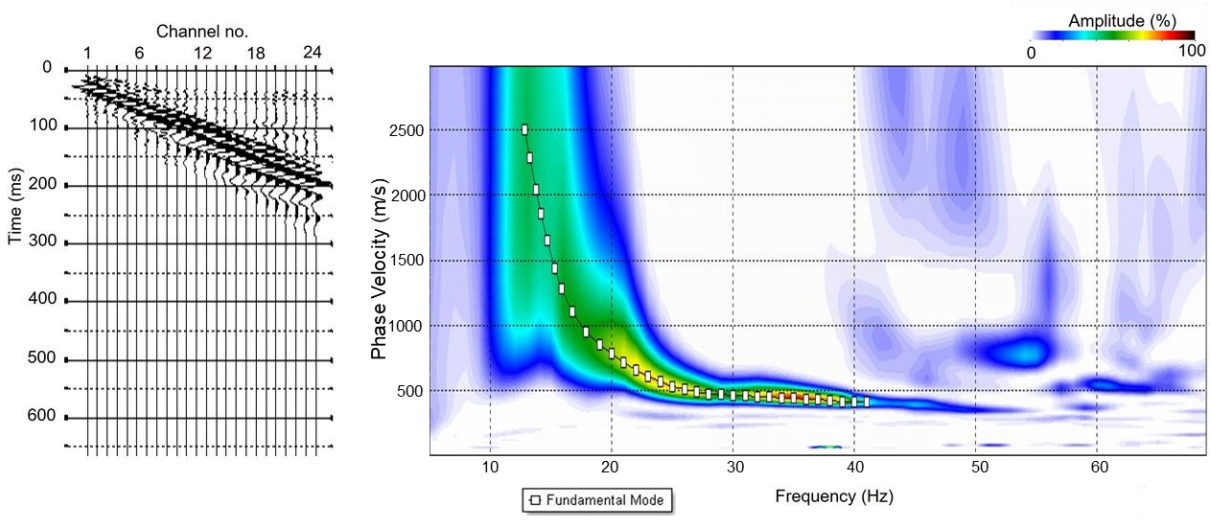

Figure 4.4: MASW data inversion

The first arrivals of the acquired surface wave data were collected and analyzed as the refraction data using the SeisImager Software (Geometrics, 2009). A nonlinear least-square method was applied to invert the travel time curves. Inversion carried out in this study included time term and tomographic inversions. The time-term inversion process generated the Vp of the subsurface at each geophone location. For tomographic inversion, an primary velocity model was created from the time-term inversion to reduce the root mean square (RMS) error among the examined and calculated travel times.

4.6 Data Interpretation

In order to streamline the interpretation of the geophysical data acquired at the embankment section of Kerr dam, the data were divided according to its locations into 1) data acquired along the top of the embankment at a ground elevation of 196 m amsl, and 2)

data acquired down the embankment at a ground elevation of 185 m amsl. The following sections provide the data interpretation for each location.

Data acquired along the top of the embankment

The S-wave reflection profile shows three subsurface layers. A strong, continuous, and coherent seismic reflector occurred at elevation 192 m amsl interpreted as the bottom of a 25 m embankment fill layer (Fig. 4.5b). The interpreted embankment fill is divided into two units: as indicated by a strong seismic reflector occurred at elevation 192 m amsl (Fig. 4.5b). This seismic reflector showed no correlation with any lithologic contrast in the available borehole logs and may have been caused by compaction contrast within the embankment fill or sudden change in moisture content. The bottom unit may have been subjected to higher compaction during the embankment construction. Underlying the interpreted embankment fill, a strong, continuous and coherent seismic reflector appeared at an average ground elevation of 175 m amsl with a gentle southward slope towards the concrete dam that becomes slightly steeper at distance mark 380 m. This layer corresponds to the limestone and chert bedrock underling the dam. The interpreted bedrock shows a steep slope at the most northern end of profile as its elevation drops approximately 12 m over 45 m horizontal distance. The seismic signature at this steep slope zone may indicate potential faulting. However, the seismic profile needs to be extended further towards the northern part of the dam to validate this interpretation.

In addition, the seismic signature of the interpreted bedrock below the embankment fill showed lateral variation in reflectivity and frequency content, which may indicate lateral

variation in either the rock composition or rock strength. A strong seismic reflector appears at an average elevation of 155 m within the interpreted bedrock which may indicate a change in bedrock lithology. None of the available borehole have penetrated deep enough to detect this lithologic change in bedrock. Studying the cores from few available boreholes in the survey area indicates a lower bedrock unit made of the crystalline limestone of St. Joe Group showing at shallower depths than the lower strong seismic reflector.

The ERT profile obtained along the crest of the embankment (Fig. 4.5c) exhibits three geoelectric layers with different resistivity contrast. The first geoelectric layer shows relatively low resistivity (<60 Ohm-m) and an average thickness of 23 m, interpreted as the embankment fill delineated along the S-wave reflection profile. The upper 5 m of the embankment fill shows slightly lower and more homogenous resistivity compared to the lower part that shows relatively higher and more variable resistivity. The second geoelectric layer occurred at elevation 185 m amsl with moderate resistivity (101 to 200 Ohm-m) and an average thickness of 6 m, interpreted as soil profile below the embankment fill. The third geoelectric layer shows relatively higher resistivity (100 to 1074 Ohm-m) and is interpreted as the bedrock, which is made up of limestone and chert of the Reeds Spring Formation. The top of the bedrock slopes gently southward towards the concrete dam.

The MASW survey along the top of the embankment generated a Vs-depth profile showing Vs variation down to elevation 155 m amsl (Fig. 4.5d). The Vs profile depicts four seismic Vs layers. The first layer has a Vs varying from 150 to 300 m/s with an average thickness of 8 m interpreted as the less compacted top layer of the embankment fill. The

second layer has Vs varying from 350 to 500 m/s occurring at elevation 190 m amsl, and with an average thickness of 10 m, interpreted as more compacted embankment fill. The third Vs layer which occurred at an average elevation of 185 m with Vs varying from 400 to 480 m/s, corresponds to the interpreted soil profile. The fourth layer has a Vs of > 550 m/s, occurring at an average elevation 175 m amsl, corresponds to the bedrock consisting of limestone and chert bedrock of the Reeds Spring Formation. The top part of the interpreted bedrock layer shows local zones with relatively low Vs between a distance mark of 40 to 120 m that may be caused by local change in lithology or fractures.

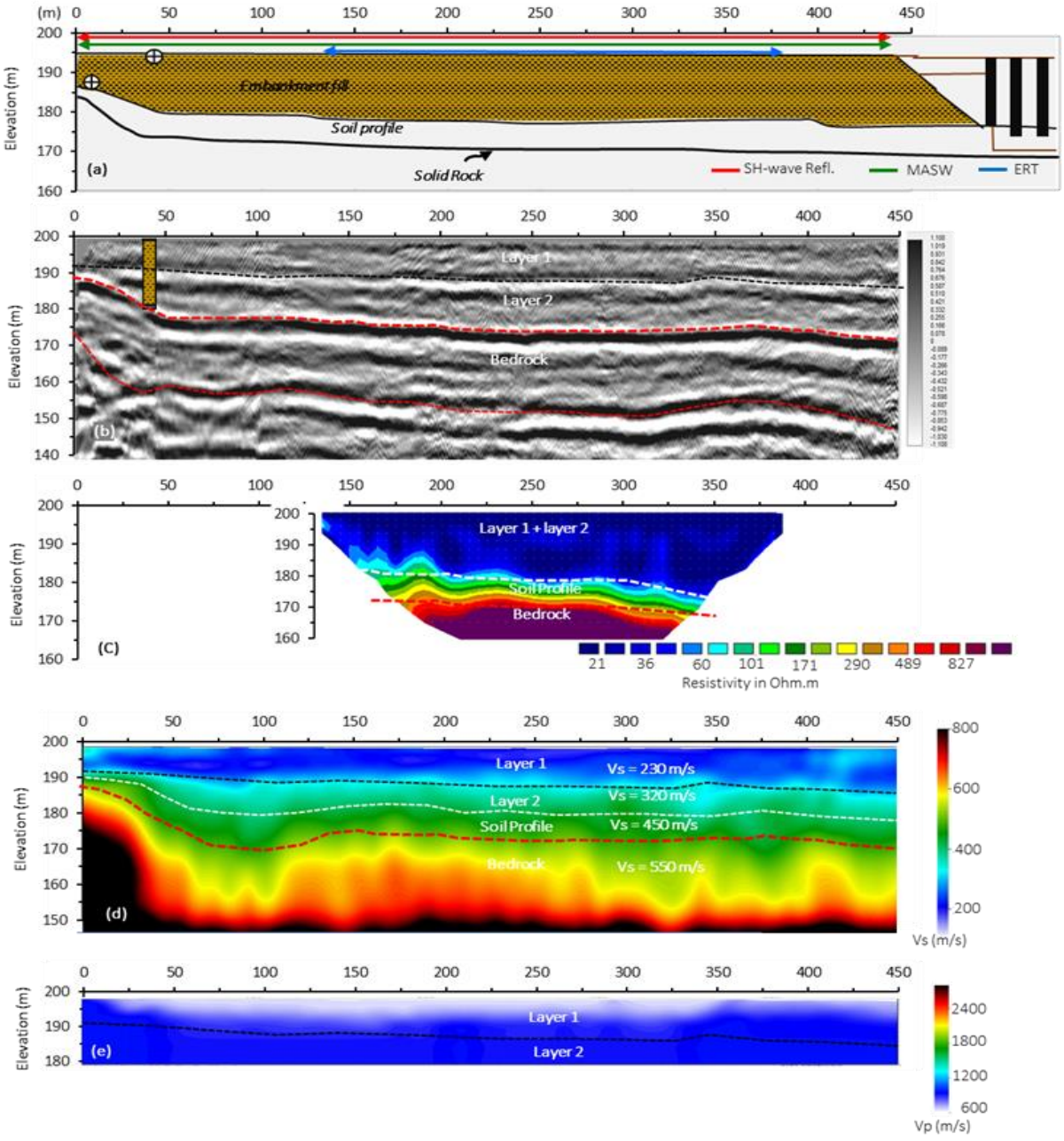

Figure 4. 5: The geophysical profiles acquired along the top of the embankment. a) Schematic drawing of the dam embankment, b) Seismic reflection profile, c) ERT profile, d) MASW profile, and e) seismic refraction profile. Interpreted S-wave seismic interfaces are superimposed on the rest of the geophysical profiles as red dashed lines. Interpreted dashed line with different color indicates the different layers on these profiles.

The seismic P-wave refraction profile acquired along the top of the embankment imaged the subsurface down to 180 m ground elevation only (Fig. 4.5e) showing a steady raise in P-wave velocity (Vp) with depth. This steady raise Vp with depth (600 to ~1000 m/s) was difficult to be characterized into separate seismic velocity layers.

Data acquired toe of the embankment

The S-wave reflection profile-2 acquired from the toe of embankment (downstream toe) (Fig. 4.6b) shows three subsurface layers. The bottom of the of the upper layer is evident by strong and coherent seismic reflector is identified at an average elevation of 175 m. The upper layer is interpreted as the surficial soil profile with a thickness of ~5-8. The bedrock layer underlying surficial soil profile (Fig. 4.6b) occurs at an average elevation of 175 m comparable to interpreted bedrock surface from seismic reflection profile obtained along the top of the embankment (Fig. 4.5b). A strong seismic reflector appears at ~20 m below the imaged bedrock surface at an average elevation of 155 m that is referred to a change in bedrock lithology. A series of discontinuous reflectors were observed within the bedrock and may indicate multiple bedding interfaces. Few distinct local features with different seismic signatures within the bedrock (Fig. 4.6b) were observed compares to that imaged by the S-wave profile acquired along the top of the embankment (Fig. 4.5b). These local features occur at distance marks 90 -170 m and 245 – 290 m along the seismic profile and may indicate lateral change in the rock stiffness. The most northern part of profile shows a steep slope and displaced reflectors that may indicate potential faulting at this location.

ERT profile acquired down the embankment imaged the subsurface to a depth of 140 m (Fig. 4.6c). The upper layer has relatively low resistivity <90 Ohm-m and an average thickness of 5 m, interpreted as the soil profile capping the bedrock surface. The second geoelectric layer occur at an average elevation of 175 m amsl, with a thickness of 20 m and resistivity values ranging from 290 to 1074 Ohm-m. This layer signifies the limestone and chert bedrock of the Reeds Spring Formation. The lateral variation in resistivity estimates and thickness of this unit is most likely caused by variation in the moisture content. A third geoelectric layer with notably low resistivity (<150 Ohm-m) appears under the limestone and chert which correlates to the second bedrock layer imaged by the nearby seismic reflection profile (Fig. 4.6c). As this layer appears along both the S-wave reflection and the resistivity profiles indicates that this layer has different lithology than the overlying limestone layer.

The MASW profile (Fig. 4.6d) shows two velocity layers. The top layer is described by a Vs varying from 200 to 300 m/s with an average thickness of 6 m which corresponds to the interpreted soil profile. The bottom layer underlying the soil profile has Vs of 600 m/s and occurs at an average elevation of 175 m which is the interpreted as the limestone bedrock of the Reeds Spring Formation. The bedrock generally showed lateral Vs variation that may indicate changes in the rock stiffness.

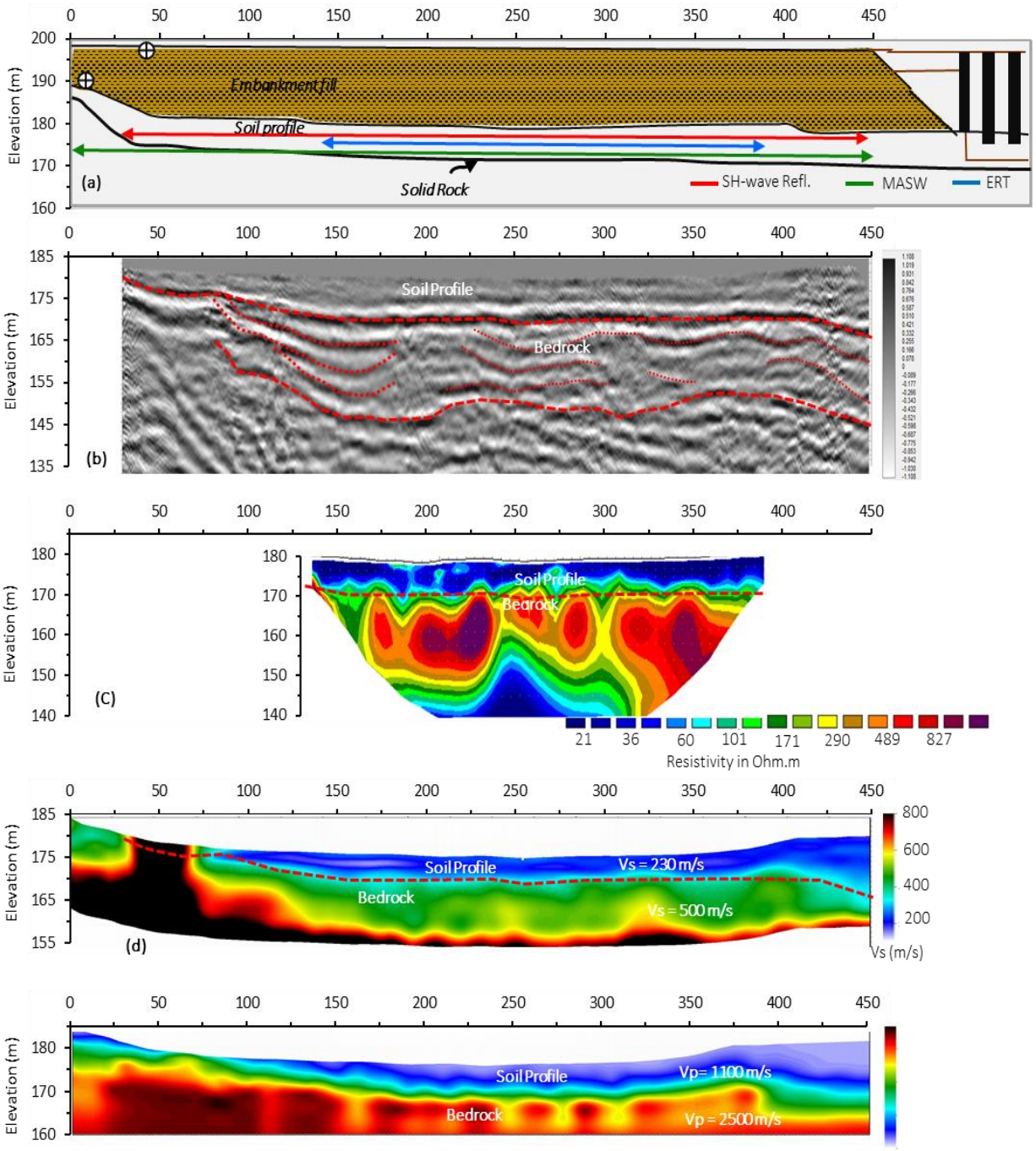

Figure 4.6: The geophysical profiles acquired along the toe of the embankment. a) Schematic drawing of the dam embankment, b) Seismic reflection profile-3, c) ERT profile-1, d) MASW profile-3 and e) Seismic refraction profile-3. Interpreted S-wave seismic interfaces are superimposed on the rest of the geophysical profiles as red dashed lines.

P-wave refraction profile shows two P-wave velocity (Vp) layers (Fig. 4.6e). The top layer has Vp varying from 600 to 1200 m/s and occurs at an average elevation of 180 m amsl, interpreted as the soil profile on the top of the bedrock surface. The bottom layer occurs at an average elevation of 175 m and has Vp ranging from 2000 to 2800 m/s, interpreted as the limestone bedrock of Reeds spring Formation.

4.7 Discussion

The integration of S-wave reflection, MASW, Seismic P-wave refraction, and ERT profiles provided a better characterization of the embankment and underlying bedrock at the dam. Overlaying the ERT and MASW profiles on top of the S-wave reflection profiles (Fig. 4.7) showed that the subsurface is characterized into three layers including the embankment fills, a soil profile, and the underlying bedrock. The embankment fill, subdivided into an upper and lower unit, exhibits low resistivity and low Vs characterized as loosely compacted gravel fill with moist clay content. The ERT profile did not differentiate between the upper and lower embankment fill units (Fig. 4.7b) compared to the S-wave reflection and MASW profiles as shown in figures 4.7b and 4.7c respectively. The geophysical profiles characterized a thin (6-8 m) soil profile underlying the embankment fill. The soil profile is characterized by moderate Vs and moderate electrical resistivity interpreted. The bedrock was characterized into two units. The upper bedrock, Reeds Spring Formation, delineated by the geophysical profiles was characterized by high Vs and high resistivity. A low Vs zone was observed within the upper bedrock unit (Fig. 4.7c) which may be because of a variation in

lithology or fractures. However, the deeper bedrock unit was only imaged by the S-wave reflection profiles. The ERT and MASW did not delineate the second bedrock because of the lack of depth of penetration and low resolution at deeper depth.

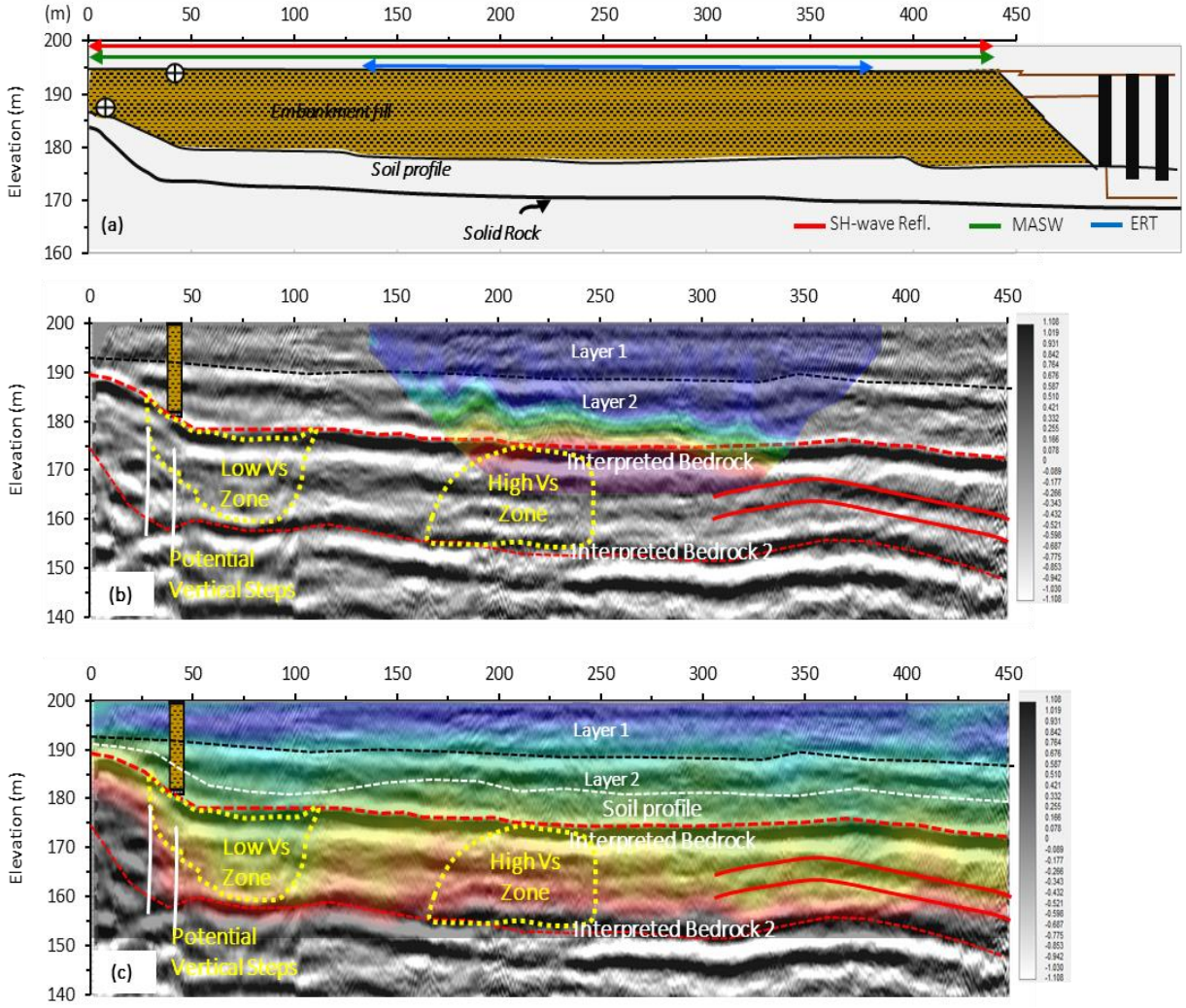

Figure 4.7: Integrated geophysical profiles along the top of the embankment. a) Schematic drawing of the dam embankment, b) superimposition of Seismic reflection profile and ERT profile, and b) superimposition of seismic reflection profile and MASW profile along the top of the embankment.

The superimposed ERT and MASW on top of the S-wave reflection profile for the toe of the embankment (Fig. 4.8) correlated well with the geophysical profiles acquired from the top of the embankment. The low resistivity and low Vs within the bedrock unit at distance marks 245 m and 305 m (Fig. 4.8b) may indicate possible zone of degradation within the bedrock. This zone may require further monitoring for possible seepage in the future. A low Vs zone identified along the S-wave reflection and the MASW profiles (Fig. 4.8c) which correlates will with the low Vs zone identified along the top of the embankment geophysical profiles. This low Vs zone (Fig. 4.8c) may be referred to local weathering of fracturing within the Reeds Spring Formation at this location.

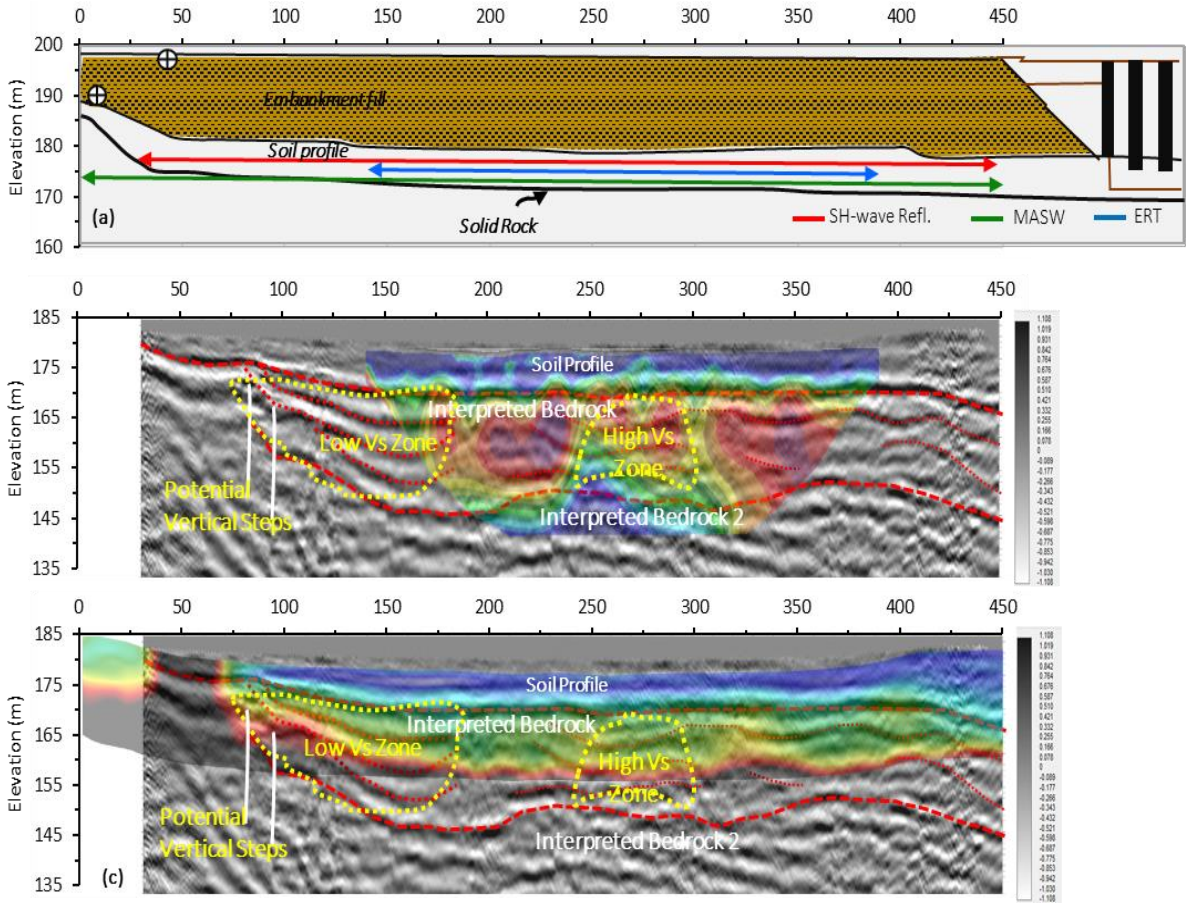

Figure 4.8: Integrated geophysical profiles along the toe of the embankment. a) Schematic drawing of the dam embankment, b) superimposition of Seismic reflection profile and ERT profile, and b) superimposition of seismic reflection profile and MASW profile along the bottom of the embankment.

The interpretations of the geophysical profiles were integrated to generate subsurface models for the dam (Fig. 4.9). The model shows the embankment fill with an average thickness of 20 m, characterized into upper and lower units. The geophysical characteristics of the upper unit of the embankment fill suggests that it may be coarse-grained embankment fill (Fig. 4.9a). However, the lower unit appears to be more compacted and possibly fine-grained embankment fill. A 6 m thick soil profile occurs beneath the embankment fill. The bedrock surface showed clearly along all the acquired geophysical profiles at an average elevation of 175 m amsl. The bedrock surface slopes gently southward toward the concrete dam (Fig. 4.9b) and shows a steep slope at the most northern part of the surveyed section. This abrupt change in slope in the detected bedrock units my cause by a local faulting at this location or possible folding extending towards the north of the profile. However, confirming this structural interpretation requires to extend the seismic profiles further north as the interpreted fault shows at the edges of the profiles. The low velocity zone within the bedrock is interpreted as comparatively weathered and fractured area near to the interpreted fault. The high velocity zone is interpreted as probably a more rigid limestone with higher concentration of chert. A second bedrock unit was imaged at an average ground elevation of 150 m. This second bedrock unit is most likely the Chattanooga Shale as it exhibits different geophysical signature compared to the overlying thinly bedded

limestone and chert of the Reed Spring Formation. No active seepage zone was identified along the surveyed section of the embankment of the dam in this study. The geophysical data were acquired during a dry season where the water level in the reservoir was relatively low. Repeating the geophysical measurements, more particularly the electric resistivity measurements, during a rainy season may detect possible seepage zones.

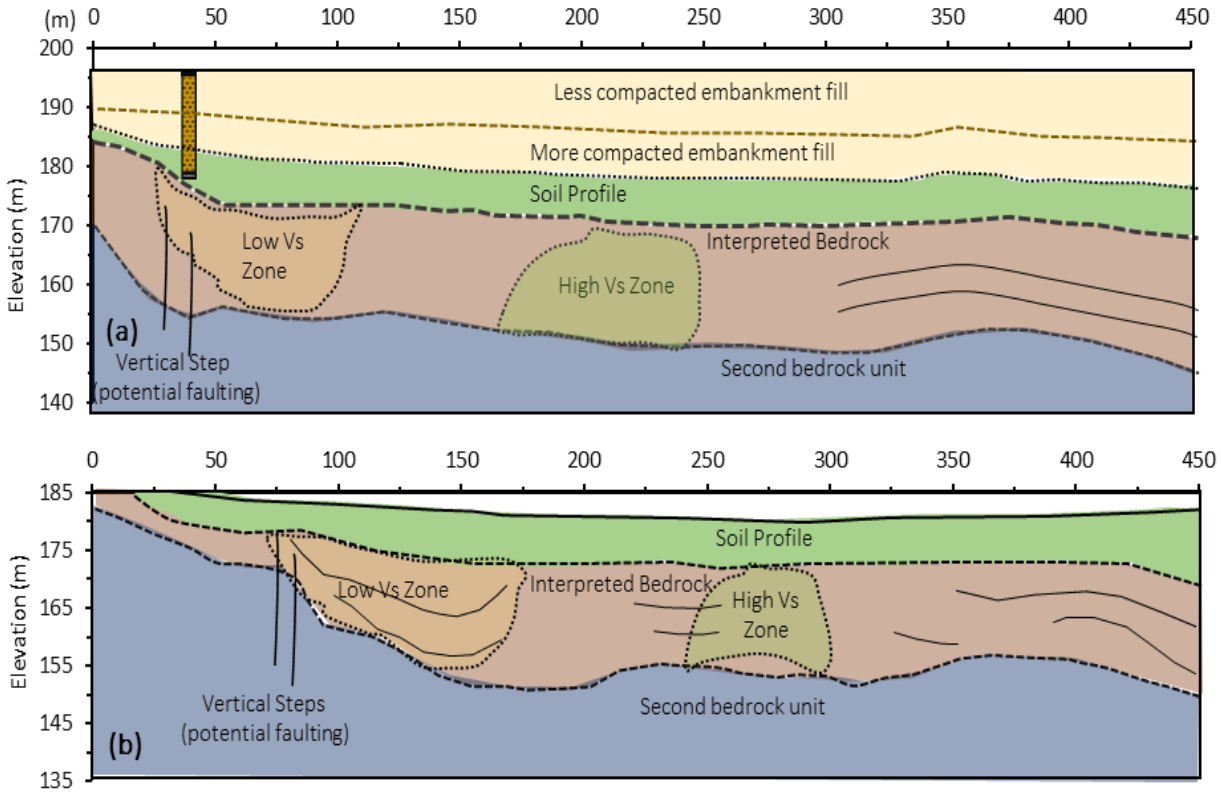

Figure 4.9: Integrated understanding of the geophysical data acquired along the top of the embankment (a) and down the embankment (b) of Kerr Dam.

The different geophysical surveys applied in this study revealed different subsurface conditions. The S-wave reflection survey provided high resolution image of the embankment

and its underlying bedrock units with nearly 60 m depth of penetration. The high-quality S-wave reflection data acquired in this research were mainly attributed to the ground surface allowed for good coupling among the land streamer system mounted geophones and the surface ground. The seismic survey was carried out along a smooth and fairly compacted top and toe of the which improved the geophone coupling, enhanced the signal to noise ratio. The ground surface conditions have also contributed to acquiring good quality MASW and seismic refraction data using the land streamer technology. For the electrical resistivity tomography (ERT) method, the results showed generally low resistivity and very little to no resistivity contrast between the upper and lower dam fill units. The low resistivity contrast within the fill materials may be attributed to the moisture of the dam fill units because of the lake water and the heavy rain on the day of survey. Nonetheless, the integration of the results of the applied geophysical methods provided a better understanding of the relatively homogenous embankment and the underlying bedrock.

4.8 Conclusion

In this study, the embankment section of the Robert S. Kerr Dam was investigated to inspect its internal structure, soil foundation and its underlying bedrock integrity utilizing a suite of geophysical techniques consisting of S-wave reflection, ERT, MASW, and P-wave refraction. Despite the usefulness of each geophysical method, their application varies largely depending on the goals of the study. The Vp measurements from the seismic refraction method can differentiate the main geological units based on their acoustic

contrast while the Vs measurements from the MASW method can offer evidence about the compaction, and stiffness condition, of the constituents regardless the influence of moisture content. Among the applied multiple geophysical methods, this study also focused on the efficacy of the integrated seismic and electrical methods as a combined approach for routine investigation and assessment of earth fill dams i.e., the embankment part of the Kerr dam. The seismic and electrical resistivity method can complement each other for investigating the rock properties and moisture content. As S-wave velocity and propagation are less affected by the moisture content, the method can provide a better depiction of the rock matrix and suggest the presence of fractures. The electrical resistivity method is more sensitive to the moisture and clay content and can detect water-filled fractures.

The integrated geophysical methods provided a detailed image of the dam body (upper and lower dam fill unit), soil foundation, and two bedrock units with different lithological properties. Low Vs anomalous zone was observed along the seismic profiles indicating lateral variation within the bedrock units. The dam body shows overall low resistivity, low Vs, and low Vp for both upper and lower dam fill unit indicating moisture and clay content. Most of the geophysical methods were able to depict the upper bedrock unit of Reed Spring Formation with a reliable agreement which is relatively flat sloping southward, however, only the S-wave reflection method was able to depict the deeper bedrock unit. Integrating multiple geophysical method seems to be capable of providing solution for temporal and routine monitoring of the embankment and its underlying foundation. On the basis of the geophysical evidence, repeating these measurements on annual or semi-annual basis will

help tracking changes in the embankment and underlying rock foundation which will contribute to the safety and long-term functioning of the dam.

References

Baker, G. S., Steeples, D. W., & Schmeissner, C. (2002). The effect of seasonal soil-moisture conditions on near-surface seismic reflection data quality. first break, 20(1).

Bièvre, G., Lacroix, P., Oxarango, L., Goutaland, D., Monnot, G., & Fargier, Y. (2017). Integration of geotechnical and geophysical techniques for the characterization of a small earth-filled canal dyke and the localization of water leakage. Journal of Applied Geophysics, 139, 1-15.

Cardarelli, E., Cercato, M., and De Donno, G., 2014. Characterization of an earth-filled dam through the combined use of electrical resistivity tomography, P-and SH-wave seismic tomography and surface wave data. Journal of Applied Geophysics 106, 87-95.

Cardarelli, E., Cercato, M., and Di Filippo, G., 2010. Geophysical investigation for the rehabilitation of a flood control embankment. Near Surface Geophysics 8(4), 287-296.

Cederstrand, J. R. (1997). Digital geologic map of Tulsa Quadrangle, northeastern Oklahoma (No. 96-380). US Geological Survey.

Chalikakis, K., Plagnes, V., Guerin, R., Valois, R., & Bosch, F. P. (2011). Contribution of geophysical methods to karst-system exploration: an overview. Hydrogeology Journal, 19(6), 1169-1180.

Choquette, P. W., Cox, A., & Meyers, W. J. (1992). Characteristics, distribution and origin of porosity in shelf dolostones; Burlington-Keokuk Formation (Mississippian), US Mid-Continent. Journal of Sedimentary Research, 62(2), 167-189.

Fay, R. O., & Friedman, S. A. (1979). The Mississippian and Pennsylvanian (Carboniferous) Systems in the United States. US Geological Survey Professional Paper.

Fell, R., Wan, C. F., Cyganiewicz, J., & Foster, M. (2003). Time for development of internal erosion and piping in embankment dams. Journal of geotechnical and geoenvironmental engineering, 129(4), 307-314.Ffig

Geometrics Inc., 2009, SeisImager/2D software manual; version 3.3, p. 257. https://geometrics.com/wp-content/uploads/2019/05/SeisImager2D_Manual_v3.3.pdf

Grand River Dam Authority (GRDA) report, 2012. Potential Failure Mode Analysis (Revision 1) for the Markham Ferry Project (P-2183).

Hickey, C. J., Römkens, M. J., Wells, R. R., and Wodajo, L., 2015. Geophysical methods for the assessment of earthen dams. In Advances in Water Resources Engineering, pp. 297-359. Springer, Cham.

Huffman, G. G. (1960). Geology of the Oklahoma Ozark Region.

Huffman, G. G., Langton, J. M., & Hancock, J. M. (1966). Geology of Northern Adair County, Oklahoma. University of Oklahoma.

Hunter, J. A., Pullan, S. E., Burns, R. A., Gagne, R. M., & Good, R. L. (1984). Shallow seismic reflection mapping of the overburden-bedrock interface with the engineering seismograph—Some simple techniques. Geophysics, 49(8), 1381-1385.

Ikard, S. J., Rittgers, J., Revil, A., and Mooney, M. A., 2015. Geophysical investigation of seepage beneath an earthen dam. Groundwater 53(2), 238-250.

Jones, G., Sentenac, P., & Zielinski, M. (2014). Desiccation cracking detection using 2-D and 3-D Electrical Resistivity Tomography: Validation on a flood embankment. Journal of Applied Geophysics, 106, 196-211.

Jongmans, D., & Garambois, S. (2007). Geophysical investigation of landslides: a review. Bulletin de la Société géologique de France, 178(2), 101-112.

Kansas Geological Survey, Surfseis MASW Software overview. https://www.kgs.ku.edu/software/surfseis/s2intro.html, 2017 (accessed 4th November 2021).

Karl, L., Fechner, T., Schevenels, M., François, S., & Degrande, G. (2011). Geotechnical characterization of a river dyke by surface waves. Near Surface Geophysics, 9(6), 515-527.

Lane, N. (2007). Aging infrastructure: Dam safety. Congressional Research Service.

Lin, C. P., Hung, Y. C., Yu, Z. H., & Wu, P. L. (2013). Investigation of abnormal seepages in an earth dam using resistivity tomography. Journal of GeoEngineering, 8(2), 61-70.

Loke, M. H., 2000. Electrical imaging surveys for environmental and engineering studies. A practical guide to 2-d and 3-d surveys, 61.

Loke, M. H., & Barker, R. D. (1996). Rapid least-squares inversion of apparent resistivity pseudosections by a quasi-Newton method1. Geophysical prospecting, 44(1), 131-152.

Mazzullo, S. J., Boardman, D. R., Wilhite, B. W., Godwin, C., & Morris, B. T. (2013). Revisions of outcrop lithostratigraphic nomenclature in the Lower to Middle Mississippian Subsystem (Kinderhookian to Basal Meramecian series) along the shelf-edge in southwest Missouri, northwest Arkansas, and northeast Oklahoma.

Miller, R. D. (1992). Normal moveout stretch mute on shallow-reflection data. Geophysics, 57(11), 1502-1507.

Morris, M., Benahmed, N., Philippe, P., Royet, P., Tourment, R., van den Ham, G., & van Beek, V. (2012). WP 3: reliability of urban flood defences—D. 3.1 Guidance on improved performance of urban flood defenses. Report Number: WP3-01-12-11.

National Inventory of Dams (NID), Carl Blackwell Dam NID data. https://nid.usace.army.mil/ords/f?p=105:113:5312634610476::NO:113,2:P113_recordid:63472, 2018 (accessed 4th November 2021).

Nwokebuihe SC, Alotaibi AM, Elkrry A, Torgashov EV, Anderson NL. 2017. Dam seepage investigation of an Earthfill dam in Warren County, Missouri using geophysical methods.

Omofunmi, O. E., Kolo, J. G., Oladipo, A. S., Diabana, P. D., & Ojo, A. S. (2017). A review on effects and control of seepage through earth-fill dam. Current Journal of Applied Science and Technology, 22(5), 1-11.

Osborn, N. I. (2001). Hydrogeologic Investigation Report of the Boone Groundwater Basin, Northeastern Oklahoma.

Putiška, R., Nikolaj, M., Dostál, I., & Kušnirák, D. (2012). Determination of cavities using electrical resistivity tomography. Contributions to Geophysics and Geodesy, 42(2), 201-211.

Sazal, Z., Ismail, A., and Sanuade, O., 2021. Geophysical investigation at Carl Blackwell Dam, Stillwater, Oklahoma. Symposium on the Application of Geophysics to Engineering and Environmental Problems Proceedings, 88-88. https://doi.org/10.4133/sageep.33-047.

Sjödahl, P., Dahlin, T., & Johansson, S. (2005). Using resistivity measurements for dam safety evaluation at Enemossen tailings dam in southern Sweden. Environmental geology, 49(2), 267-273.

Steeples, D. W., & Miller, R. D. (1998). Avoiding pitfalls in shallow seismic reflection surveys. Geophysics, 63(4), 1213-1224.

Stumpf, A. J., & Ismail, A. (2013). High-resolution seismic reflection profiling: an aid for resolving the Pleistocene stratigraphy of a buried valley in central Illinois, USA. Annals of Glaciology, 54(64), 10-20.

Telford, W. M., Telford, W. M., Geldart, L. P., & Sheriff, R. E. (1990). Applied geophysics. Cambridge university press.

Woolery, E. W., 2018. SH-Mode Seismic-Reflection Imaging of Earthfill Dams. Engineering 4(5), 694-701. https://doi.org/10.1016/j.eng.2018.08.009.

Yilmaz, Ö. (2001). Seismic data analysis: Processing, inversion, and interpretation of seismic data. Society of exploration geophysicists.

Zhang, L. M., & Chen, Q. (2006). Seepage failure mechanism of the Gouhou rockfill dam during reservoir water infiltration. Soils and Foundations, 46(5), 557-568.

VITA

Md Zonaed Hossain Sazal

Candidate for the Degree of

Doctor of Philosophy

Dissertation: GEOPHYSICAL CHARACTERIZATIONS OF GLACIAL AQUIFERS AND EARTH-FILL DAMS

Major Field: Geology

Biographical:

Education:

Completed the requirements for the Doctor of Philosophy in Geology at Oklahoma State University, Stillwater, Oklahoma in May, 2022.

Completed the requirements for the Master of Science in Geophysics at University of Dhaka, Dhaka, Bangladesh in 2014.

Completed the requirements for the Bachelor of Science in Geology at University of Dhaka, Dhaka, Bangladesh in 2011.

Experiences:
Environmental and geotechnical site characterization, dam sites investigation, and aquifer characterization using multiple geophysical methods. Experienced in field acquisition, data processing, report writing, presentations, and project deliverables. Nearly 5 years of teaching experience at Boone Pickens School of Geology as a Graduate Teaching Associate and 1-year experience in consultation at the Writing Center of Oklahoma State University.

Professional Memberships:
Society of Exploration Geophysics (SEG), American Association of Petroleum Geologist (AAPG), Geological Society of America (GSA)